Arabian Journal of Chemistry (2018) xxx, xxx–xxx

King Saud University

Arabian Journal of Chemistry

www.ksu.edu.sa
www.sciencedirect.com

ORIGINAL ARTICLE

Electrocatalytic urea mineralization in aqueous alkaline medium using Ni^{II}cyclam-modified nanoparticulate TiO_2 anodes and its relationship with the simultaneous electrogeneration of H_2 on Pt counterelectrodes

S. Murcio-Hernández [a], A.V. Rueda-Solorio [a], J.A. Banda-Alemán [a], C. González-Nava [a], F.J. Rodríguez [a], E. Bustos [a], F. Espejel-Ayala [a], A. Rodríguez [a], S. Sepúlveda [b], J. Manríquez [a,*]

[a] *Centro de Investigación y Desarrollo Tecnológico en Electroquímica S.C., Parque Tecnológico Querétaro s/n, Sanfandila, 76703, Pedro Escobedo, Querétaro, Mexico*
[b] *Centro de Innovación, Investigación y Desarrollo en Ingeniería y Tecnología, Universidad Autónoma de Nuevo León, Nuevo León, Mexico*

Received 9 October 2017; accepted 24 December 2017

KEYWORDS

Ni^{II}cyclam electrodeposition;
Nanoparticulate TiO_2 electrodes;
Urea mineralization;
CO intermediates inhibition;
H_2 electrogeneration

Abstract Ni^{II}cyclam-modified nanoparticulate TiO_2-coated ITO electrodes (ITO/TiO_2//Ni^{II}-cyclam) were prepared by electropolymerization of Ni^{II}cyclam monomers to TiO_2-coated ITO electrodes (ITO/TiO_2) to improve electrocatalytic urea $CO(NH_2)_2$ oxidation in alkaline aqueous solutions. A high value adding secondary effect was the collection of electrons at Pt cathodes, to simultaneously generate H_2 from water reduction. Ni^{II}cyclam-modified ITO electrodes (ITO//Ni^{II}-cyclam) were also prepared by electropolymerization of Ni^{II}cyclam monomers to bare ITO electrodes (ITO) for comparison purposes. In the presence of the TiO_2 nanoparticles, the urea mineralization on Ni^{II}cyclam coatings was doubled (23.95% – organic carbon removal at 120 min of electrolysis) compared to those without TiO_2 nanoparticles (13.02% – organic carbon removal at 120 min of electrolysis).

In agreement, the faradaic efficiency for H_2 generation at the Pt cathode, electrically connected to an anode having TiO_2 nanoparticles (0.99 at 120 min of electrolysis), was also twice as effective than

* Corresponding author.
E-mail address: jmanriquez@cideteq.mx (J. Manríquez).
Peer review under responsibility of King Saud University.

Production and hosting by Elsevier

https://doi.org/10.1016/j.arabjc.2017.12.029

Please cite this article in press as: Murcio-Hernández, S. et al., Electrocatalytic urea mineralization in aqueous alkaline medium using Ni^{II}cyclam-modified nanoparticulate TiO_2 anodes and its relationship with the simultaneous electrogeneration of H_2 on Pt counterelectrodes. Arabian Journal of Chemistry (2018), https://doi.org/10.1016/j.arabjc.2017.12.029

that observed when the same Pt cathode was electrically connected to an anode without TiO_2 nanoparticles (0.46 at 120 min of electrolysis). The experimental results indicated that the poisoning of Ni^{II} centers (which is caused by an excessive production of CO intermediates during the urea oxidation on both Ni^{II}cyclam-modified anodes) was strongly inhibited in the presence of the nanoparticulate TiO_2|Ni^{II}cyclam junction.

A final comparison between our results and those reported in selected publications revealed that the Ni^{II}cyclam-modified nanoparticulate TiO_2-coated ITO anodes here developed, constitutes a promising electrocatalytic system for performing direct urea mineralization at a relative short electrolysis time. Furthermore, the combination of the following phenomena: (a) effective charge separation on the semiconducting ITO|nanoparticulate TiO_2 junctions, (b) remarkable capabilities of the nanoporous TiO_2 films for tuning the load of OH^- anions demanded by the urea oxidation and, (c) outstanding capabilities of the TiO_2 nanoparticles for capturing CO intermediates (at Ti^{3+} donor sites), successfully promoted the enhancement of the electron external transport to Pt cathodes, and consequently improved the faradaic efficiency associated to the cathodic generation of H_2.

1. Introduction

Urea $CO(NH_2)_2$ has attracted the attention of the worldwide research groups because these molecules have been identified as viable hydrogen (H_2) carriers (Rollinson et al., 2011). Therefore, studies of electrochemical oxidation processes of urea are essential for developing promising technologies for H_2 production (Eq. (1)) through direct (Boggs et al., 2009; King and Botte, 2011) or solar driven (Kim et al., 2012, 2013; Wang et al., 2012; Cho and Hoffmann, 2014) urine electrolysis. In particular, urea oxidation in aqueous alkaline medium has been electrocatalytically promoted on NiO(OH)-modified anodes (according to Eqs. (2) and (3)) in order to collect electrons which are immediately conducted to a Pt cathode through the external wiring where the H_2 evolution is achieved from the electro-reduction of H_2O (see Eq. (4)) (Boggs et al., 2009; King and Botte, 2011; Kim et al., 2012, 2013; Wang et al., 2012; Cho and Hoffmann, 2014).

$$CO(NH_2)_2 + H_2O \rightarrow N_2 + 3H_2 + CO_2 \quad (1)$$

$$Ni(OH)_2 + OH^- \rightarrow NiO(OH) + H_2O + e^- \quad (2)$$

$$CO(NH_2)_2 + 6OH^- \rightarrow N_2 + 5H_2O + CO_2 + 6e^- \quad (3)$$

$$6H_2O + 6e^- \rightarrow 3H_2 + 6OH^- \quad (4)$$

To better understand the reaction mechanism of the urea oxidation in the presence of the NiO(OH), Botte et al. carried out Tafel studies (Vedharathinam and Botte, 2012) and surface enhanced Raman spectroscopy (Vedharathinam and Botte, 2013, 1812). Their results demonstrated that high concentrations of urea molecules (e.g. 0.2–1.0 M) are oxidized by NiO(OH) with an electrochemical-chemical (EC) mechanism (see Eqs. (5) and (6)), exhibiting reaction orders of 2 and 0.3, corresponding to OH^- ions and urea concentrations, respectively (Vedharathinam and Botte, 2012; Díaz-Morales et al., 2016). Consequently, the reaction rate at 0.45 V vs. Ag|AgCl was not dependent on the urea molecules concentration, however, the NiO(OH) electrocatalyst must be electrochemically regenerated n-times (see Eq. (5)) (Díaz-Morales et al., 2016) to achieve up to 13% degradation, transferring 3(n − 1) electrons per urea molecule (see Eq. (6), where n = 3) during urea electrolysis for 22 h (Boggs et al., 2009; Fleischmann et al., 1971; Daramola et al., 2010). This mechanism is also interesting because the reaction order of 2 for the OH^- ions concentration strongly suggests that both C-NH_2 groups of the urea molecule are chemically oxidized by one electrocatalytic site containing two electrodeposited Ni^{III} atoms (Daramola et al., 2010). These kinetic conditions reflect the oxidation mechanism of urea on Pt(100)-oriented electrodes (Climent et al., 1997, 2001; Pierozynski et al., 1999), or the oxidation of organic compounds at an anodized nickel electrode in an alkaline solution (Fleischmann et al., 1971).

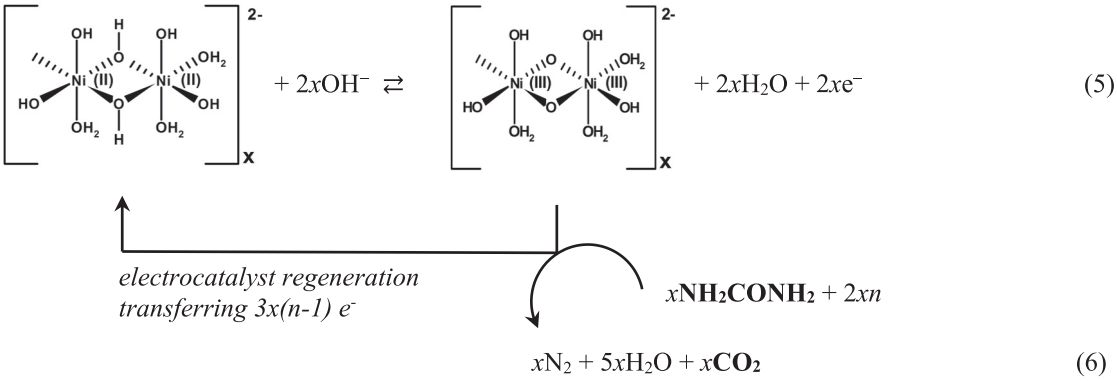

(5)

(6)

Please cite this article in press as: Murcio-Hernández, S. et al., Electrocatalytic urea mineralization in aqueous alkaline medium using Ni^{II}cyclam-modified nanoparticulate TiO_2 anodes and its relationship with the simultaneous electrogeneration of H_2 on Pt counterelectrodes. Arabian Journal of Chemistry (2018), https://doi.org/10.1016/j.arabjc.2017.12.029

The application of higher anodic potentials (where generation of **Ni^{III} sites** is predominant) promotes the O_2 evolution reaction via Eq. (7), however, it also deactivates a fraction of the NiO(OH) electrocatalyst (Díaz-Morales et al., 2016; Casella et al., 1993). Therefore, it is reasonable to propose that alternative Ni(II) electrocatalysts could be combined with other electrode materials to activate the urea oxidation, by inhibiting the Eq. (7), at higher potentials, e.g. 0.6–0.8 V vs. Ag|AgCl.

$$2\ NiO(OH) \rightarrow 2\ NiO + 2\ {}^{\bullet}OH \rightarrow \tfrac{1}{2}\ O_2 + H_2O$$
$$+\ 2OH^-,\ 2e^- \qquad (7)$$

NH_2 groups on soluble Ni(II) complexes containing **Ni^{III} sites** (Kozitsina et al., 2009). Others that urea oxidation on these electrodes can be accomplished by following Eq. (11). There $[O–Ni^{II}L\sim\mathbf{Ni^{III}(OH)L}–O]^{3+}$ correspond to electropolymerized Ni^{III} sites on the electrode surface (McAuley and Xu, 1992) (more details on this reaction pathway can be found in the Supplementary Data SD-1).

Specifically, electropolymerized **Ni^{III} sites** can be activated on **Ni^{II}cyclam**-modified electrodes by following Eqs. (8)–(10), where the comproportionation equilibrium (Eq. (10)) requires a comproportionation constant $K_{com,film} = \exp(E^{\circ\prime}_{ox2,film} - E^{\circ\prime}_{ox1,film})F/RT$) (Taraszewska et al., 1998). Thus, the proposed urea oxidation reaction (Eq. (11)) resembles the urea oxidation on Ni(II) porphyrins-modified glassy carbon electrodes (Malinski et al., 1991; Bukowska et al., 1996; Alatorre-Ordaz et al., 1998).

$$[O–Ni^{II}L\sim Ni^{II}L–O]^{3+} + OH^- \rightleftarrows [O–\mathbf{Ni^{III}(OH)L}\sim Ni^{II}L–O]^{3+} + e^- \qquad E^{\circ\prime}_{ox1,film} \qquad (8)$$

$$[O–\mathbf{Ni^{III}(OH)L}\sim Ni^{II}L–O]^{3+} + OH^- \rightleftarrows [O–\mathbf{Ni^{III}(OH)L}\sim\mathbf{Ni^{III}(OH)L}–O]^{3+} + e^- \qquad E^{\circ\prime}_{ox2,film} \qquad (9)$$

$$[O–Ni^{II}L\sim Ni^{II}L–O]^{3+} + [O–\mathbf{Ni^{III}(OH)L}\sim\mathbf{Ni^{III}(OH)L}–O]^{3+} \rightleftarrows 2[O–Ni^{II}L\sim\mathbf{Ni^{III}(OH)L}–O]^{3+} \qquad K'_{com,film} \qquad (10)$$

electrocatalyst regeneration

$$x\mathbf{NH_2CONH_2} + 4xOH^- \rightarrow xN_2 + 3xH_2O + x\mathbf{CO_2} \qquad (11)$$

Urea electrooxidation has also been promoted in aqueous alkaline medium using Ni(II) tetraazamacrocycles complexes in solution (Casella et al., 1993) or electropolymerized films on convectional glassy carbon electrodes (Kozitsina et al., 2009; Manriquez et al., 1999; Ferrer et al., 2003). It has been reported that the oxidation of organic molecules containing C-OH or C-NH_2 groups (e.g. phenols, primary or secondary aliphatic alcohols, urea or hydrazine) by Ni(II) tetraazamacrocyles complexes including **Ni^{II}cyclam**, Ni^{II}-tmdbta and Ni^{II}salen is electrocatalytically viable in a wide range of concentrations from 20 μM to 0.1 M (Manriquez et al., 1999; Ferrer et al., 2003; Liu, 2004; Zhang et al., 2015).

It is well known that the electrocatalytic oxidation of primary C-OH groups on Ni(II) tetraazamacrocycle complexes-modified electrodes proceeds through a mechanism exhibiting reaction orders of 2 and 1, corresponding to OH^- ions and alcohol concentrations, respectively (Liu, 2004). However, the published information on the reaction mechanisms for the urea oxidation is very limited [see, for example Climent et al., 2001; Kozitsina et al., 2009; Pierozynski, 2013]. Some authors have suggested that the oxidation of urea in aqueous alkaline solution should begin by electroactivation of their

where:

an electropolymerized site $[O–Ni^{II}L\sim\mathbf{Ni^{III}(OH)L}–O]^{3+}$ =

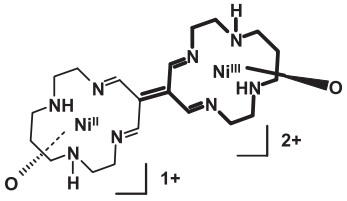

and a **Ni^{II}cyclam** monomer =

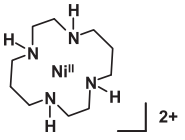

Several alternative investigations have been carried out to understand the electrocatalytic behaviour of alternative anode materials on the electrochemical oxidation of molecules such as hydrazine and urea. In these, the surfaces of conventional

Please cite this article in press as: Murcio-Hernández, S. et al., Electrocatalytic urea mineralization in aqueous alkaline medium using Ni^{II}cyclam-modified nanoparticulate TiO_2 anodes and its relationship with the simultaneous electrogeneration of H_2 on Pt counterelectrodes. Arabian Journal of Chemistry (2018), https://doi.org/10.1016/j.arabjc.2017.12.029

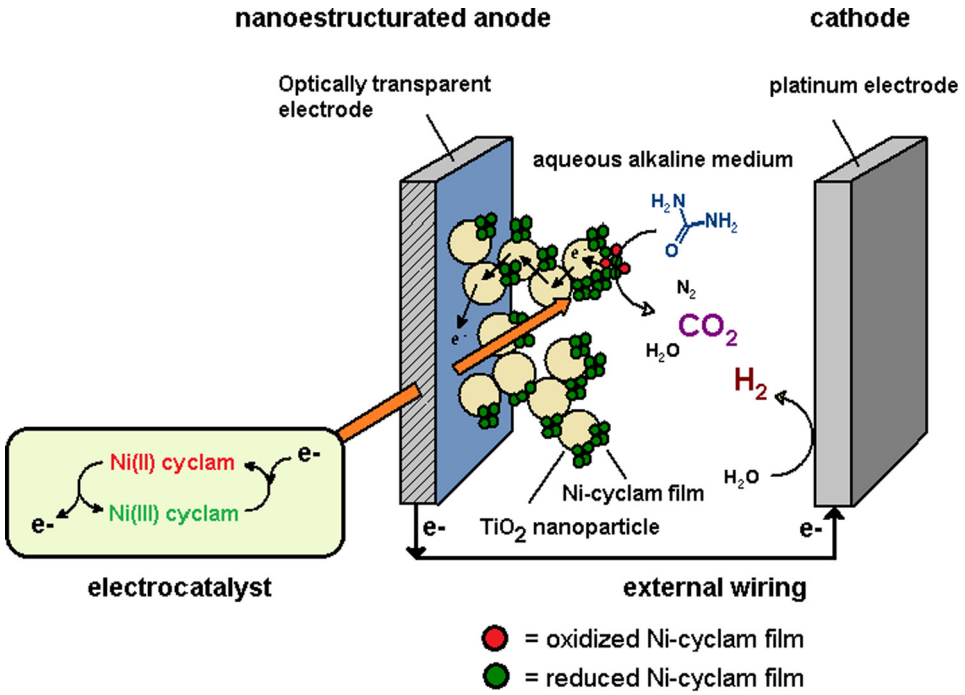

Scheme 1 Representation of the electrochemical cell proposed to conduct studies on urea electrolysis (anode, via Eq. (11)) and simultaneous H_2 generation (cathode, via Eq. (12)).

electrodes have been modified by nickel derivatives such as nickel hexacyanoferrate@TiO_2 core-shell nanoparticles (Sophia et al., 2012), Y-type zeolite-encapsulated Ni^{II}salen complexes (Zhang et al., 2015), and mercaptomethyl-terminated trinuclear Ni(II) complexes (Gu et al., 2016) to study hydrazine oxidation. Additionally, nanosheets, nanoribbons and nanowires of $Ni(OH)_2$ (Wang et al., 2011, 2012; Guo et al., 2015), Pt-Ni, Pt-Ir-Ni, Rh-Ni, Ni-Co and Ni_3N coatings (King and Botte, 2011; Yan et al., 2012; Miller et al., 2012; Liu et al., 2017), graphene oxide-Ni nanocomposites (Wang et al., 2013), $Ni(OH)_2$-$NiMoO_4{\cdot}xH_2O$ nanocomposites (Liang et al., 2015), and Ti/Pt, Ti/Pt-Ir coatings (Simka et al., 2007), have been utilized for investigating the direct electrocatalytic oxidation of urea.

A more detailed review of these references revealed that semiconductor surfaces such as RuO_2-coated DSA® electrodes (Hernlem, 2005) and Ti electrodes coated by IrO_2, RuO_2, RuO_2-TiO_2, RuO_2-TiO_2-IrO_2 or Ta_2O_5-IrO_2 (Simka et al., 2007; Hernlem, 2005; Amstutz et al., 2012), have been useful for improving urea decomposition in aqueous media. Consequently, in this investigation we propose that the physicochemical properties of very accessible oxide semiconductor electrodes such as indium-doped SnO_2 (ITO) (Hassanzadeh et al., 2004; Chowdhury et al., 2011; Plá et al., 2013), and nanoparticulate Degussa P25® TiO_2 films electrophoretically deposited on ITO electrodes (Manríquez and Godínez, 2007; Acevedo-Peña et al., 2010), could be combined, in novel ways, with the electrocatalytic capabilities of the electropolymerized **Ni^{II}cyclam** complexes (Eqs. (8)–(10)) for enhancing the urea mineralization in alkaline aqueous media (Eq. (11)). This strategy is reasonably supported by considering that the Ti-OH groups localized on the Degussa P25® TiO_2 surface (4.8 OH nm^{-2}) (Mueller et al., 2003) can be deprotonated in a highly alkaline (pH 13) aqueous solution as the point of zero charge (p.z.c.) for a TiO_2/water interface is 7.5 (Fernández-Nieves and Richter, 1998). Thus, one can expect a tuned urea oxidation rate, on electropolymerized Ni^{II}cyclam-modified nanoparticulate TiO_2 anodes, in the presence of the Ti-O^- groups, as these charged groups could reduce the entry of an excess of OH^- anions into the porous TiO_2 electrodes. To confirm this effect, one would expect a significant decrement in the total organic carbon (TOC), measured in the bulk electrolyte, between those taken before and after urea electrolysis using Ni^{II}cyclam-modified nanoporous TiO_2 anodes.

Furthermore, in this work we propose that the H_2 evolution can be simultaneously and efficiently promoted on a polycrystalline Pt cathode inserted in the same electrolysis cell, while the urea oxidation is carried out on a Ni^{II}cyclam-modified nanoparticulate TiO_2 anode (see Scheme 1). To achieve this goal, all of those electrons which were extracted from the urea molecules at the anode should be immediately transported (through external wiring) to the Pt cathode, where gaseous H_2 would be generated from the electroreduction of H_2O (see Eq. (12)) (Bratsch, 1989).

$$2H_2O + 2e^- \rightarrow \mathbf{H_2} + 2OH^- \quad E^{\circ}_{H2O|H2} = -1.02\ V\ vs.\ Ag|AgCl \tag{12}$$

2. Experimental studies

2.1. Preparation of nanoparticulate TiO_2-coated ITO electrodes

A 5.2 ± 0.7 μm thick layer of nanoparticulate TiO_2 was deposited on ITO anodes (ITO/TiO_2, this layer was measured using a Dektak 6 M Stylus profiler). The coated anodes were

Please cite this article in press as: Murcio-Hernández, S. et al., Electrocatalytic urea mineralization in aqueous alkaline medium using Ni^{II}cyclam-modified nanoparticulate TiO_2 anodes and its relationship with the simultaneous electrogeneration of H_2 on Pt counterelectrodes. Arabian Journal of Chemistry (2018), https://doi.org/10.1016/j.arabjc.2017.12.029

prepared by the electrophoretic deposition of TiO_2 nanoparticles (Degussa P25®, 21 nm diameter) on optically transparent electrodes (OTEs) based on In-doped SnO_2 (ITO, TEC15, Hartford Glass Co., USA, $\rho = 1.5 \times 10^{-3}\,\Omega\,cm$), held in a 2.23 V cm^{-1} electric field for 80 s, as previously described by our research group (Manríquez and Godínez, 2007; Pérez-Viramontes et al., 2014). The as prepared TiO_2 coated anodes were annealed in air at 450 °C for 30 min before their use. A roughness factor (R_f) of 820 ± 47 was estimated by cyclic voltammetry (CV) as previously reported (more details can be found in Supplementary Data SD-2) (Pérez-Viramontes et al., 2014). Finally, the nanoporous morphology of these electrodes was confirmed with a FEI Nova NanoSEM 200® high-resolution scanning electron microscope, HR-SEM, with accelerating voltages of 10 or 15 kV that were selected according to the characteristics of each sample.

2.2. Synthesis of Ni^{II}cyclam electrocatalyst

The Ni(II)-1,4,8,11-tetrazacyclotetradecane (**Ni^{II}cyclam**) was synthesized following a modification in the reported methodology (Bosnich et al., 1965). Here, 25.5 mg of 1,4,8,11-tetrazacyclotetradecane (98% cyclam, Strem Chemicals) and 46.9 mg of $NiCl_2{\cdot}6H_2O$ (Golden Bell, Mexico, reagent grade) were loaded in a dry 25-mL flask ball. Immediately thereafter 10 mL of absolute ethanol (J.T. Baker) was slowly added to the powders at 4 °C. A mauve raw precipitate should be observed at the bottom of the flask. The resulting mixture was refluxed for 15 min under magnetic stirring. The remnants of the initial powders and the mauve raw precipitate were entirely dissolved. After reflux was complete, and the flask content returned to room temperature, the raw product was stored in a freezer at −2 °C overnight. The mauve precipitate was filtered and washed with cooled methanol (J.T. Baker, HPLC grade) at 4 °C. After processing, the reaction yield was estimated to be 56%. The as prepared Ni^{II}cyclam complex was dried in darkness in a Petri dish before characterization by Fourier-transformed infrared spectroscopy (FT-IR) with a Nexus® Thermo-Nicolet Fourier-transform Infrared Spectrometer, and by Raman Spectroscopy (RS) using a DXR® Thermo-Scientific Dispersive Raman Microscope equipped with a 10 mW-power 532 ± 1 nm laser and a 10 × objective, and finally by UV–Vis spectroscopy (UV–Vis) in our USB2000 + F0009 Ocean Optics UV–Vis spectrophotometer (2 nm resolution). More details about the results of FT-IR, RS and UV–Vis characterization are presented in the Supplementary Data SD-3).

2.3. Preparation of Ni^{II}cyclam-modified nanoparticulate TiO_2-coated ITO electrodes

The nanoparticulate TiO_2-coated ITO electrodes (system ITO/TiO_2) were electrochemically modified with Ni^{II}cyclam to develop the electrode system: TiO_2-bearing anode (**ITO/TiO_2//Ni^{II}cyclam**) using cyclic voltammetry (CV). This technique was performed at 25 °C with an Epsilon® BASi potentiostat-galvanostat connected to a three-electrode cell containing an aqueous solution of 0.1 M NaOH (Aldrich, ≥98%) plus 2 mM Ni^{II}cyclam monomers (Kozitsina et al., 2009). Naked ITO electrodes were also coated with Ni^{II}cyclam to develop an electrode system: non-TiO_2-bearing anode (**ITO//Ni^{II}cyclam**) for comparison purposes. The working electrode systems (ITO/TiO_2 or naked ITO), an Ag|AgCl 3 M NaCl reference electrode and a Pt wire counter-electrode were immersed into the Ni^{II}cyclam containing solution for performing the coating process. During this process the interfacial potential was cycled, over 20 consecutive scans, between open-circuit-potential (o.c.p.) and 0.9 V at 25 mV s^{-1}. Apparent coverages for Ni^{II}cyclam coatings on the targeted electrodes ($\Gamma_{Ni\text{-}cyclam}$) were estimated by means of CV utilizing a similar three-electrode arrangement, but now in an aqueous solution of 0.1 M NaOH without any Ni^{II}cyclam monomers. Subsequently, Ni^{II}cyclam electropolymerization was also confirmed by elemental analysis at the outer face of the ITO/TiO_2//Ni^{II}-cyclam and ITO//Ni^{II}cyclam electrodes by means of energy-dispersive X-ray spectroscopy (EDS) using a Jeol JSM-6510LV® scanning electron microscope (SEM), at 15 kV-accelerating voltage equipped with a Bruker XFlash6I10® EDS detector (see Supplementary Data SD-4 for details). The chemical structure of the electropolymerized Ni^{II}cyclam electrocatalysts on the working electrodes, and its stability in aqueous 0.1 M NaOH, were confirmed by means of FT-IR spectroscopy employing a Nexus® Thermo-Nicolet infrared spectrometer equipped with an accessory of specular reflection, UV–Vis spectroscopy employing a USB2000 + F0009 Ocean Optics UV–Vis spectrophotometer equipped with a R400-7-UV/Vis reflection/backscattering probe, and finally, cyclic voltammetry in aqueous 0.1 M NaOH. See Supplementary Data SD-5 for detailed results.

2.4. Urea oxidation on ITO/TiO_2//Ni^{II}cyclam and ITO//Ni^{II}cyclam electrodes

Urea oxidation on **ITO/TiO_2//Ni^{II}cyclam** or **ITO//Ni^{II}cyclam** anodes (as the working electrodes, **WE**) was studied by means of cyclic voltammetry (CV), chronoamperometry (CA) and electrochemical impedance spectroscopy (EIS) techniques. CA was performed utilizing two Epsilon® BASi potentiostat-galvanostat (**P1** and **P2**), which were connected to a four-electrode cell equipped with two Ag|AgCl 3 M NaCl reference electrodes (**RE1** and **RE2**, see Scheme 2A), containing a deoxygenated aqueous solution of 0.1 M NaOH plus 10 mM urea (Sigma 99%) at 25 °C. Here the first potentiostat (**P1**, operated in three-electrode mode) was connected to the **WE** (ITO/TiO_2//Ni^{II}cyclam or ITO//Ni^{II}cyclam electrode systems), a polycrystalline Pt foil (Premion® Alfa Aesar, 25 × 25 mm, 0.5 mm-thickness) cathode (**CE**) and a reference electrode (**RE1**). Complementarily, to record the shift of the cathodic potential when the **WE** was continuously perturbed by a set of single potential-steps, the second potentiostat (**P2**, operated in two-electrode mode) was connected to another reference electrode (**RE2**) and the same **CE**.

When studying CV and EIS techniques a typical three-electrode arrangement (see Scheme 2B) was used. For this, **RE2** and **P2** were disconnected from the **CE**. CV experiments were performed with only **P1**, to scan the interfacial potential of the **WE** anodes. EIS experiments were performed with an IM6® Zahner-Elektric potentiostat-galvanostat (**P3**), to apply a sinusoidal A.C. potential (amplitude ±10 mV) to the **WE** anodes. This signal was overlapped to a set of D.C. potentials having intensities identical to the single potential-steps previously employed during CA experiments. All EIS spectra were obtained by varying the frequency of the sinusoidal A.C. per-

Please cite this article in press as: Murcio-Hernández, S. et al., Electrocatalytic urea mineralization in aqueous alkaline medium using Ni^{II}cyclam-modified nanoparticulate TiO_2 anodes and its relationship with the simultaneous electrogeneration of H_2 on Pt counterelectrodes. Arabian Journal of Chemistry (2018), https://doi.org/10.1016/j.arabjc.2017.12.029

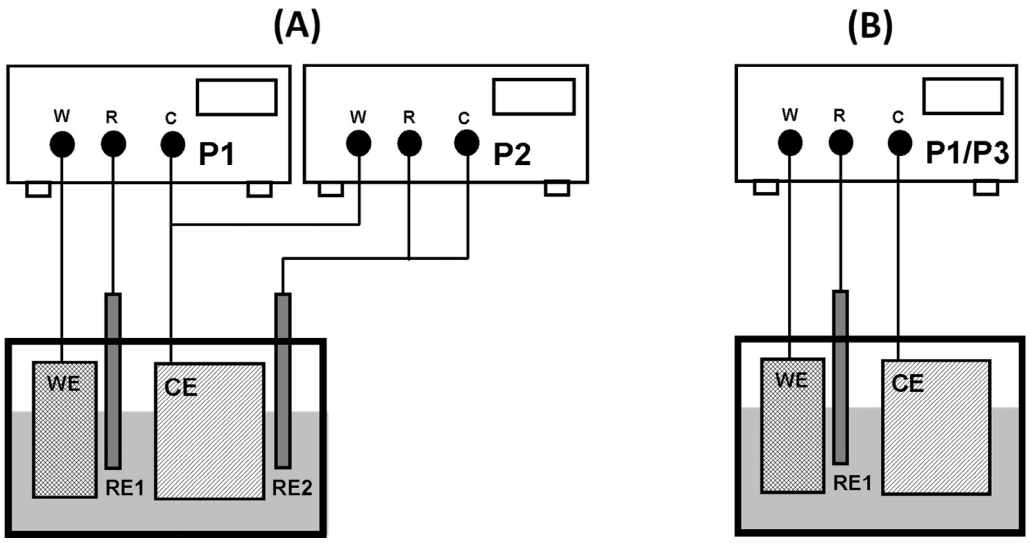

Scheme 2 Schematic arrangements for studying urea oxidation on ITO/TiO_2//Ni^{II}cyclam or ITO//Ni^{II}cyclam working-electrodes (WE) in aqueous 0.1 M NaOH. (A) CA was performed using potentiostats P1 (circuit WE-RE1-CE) and P2 (circuit CE-RE2), and (B) CV and EIS were performed using potentiostats P1 or P3, respectively, both operating in a typical three-electrode configuration.

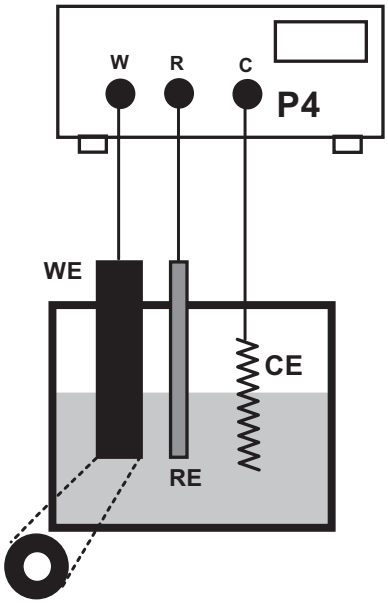

Scheme 3 Schematic arrangement employed for studying H_2O reduction on a Pt-disk working-electrode (WE) immersed in aqueous 0.1 M NaOH.

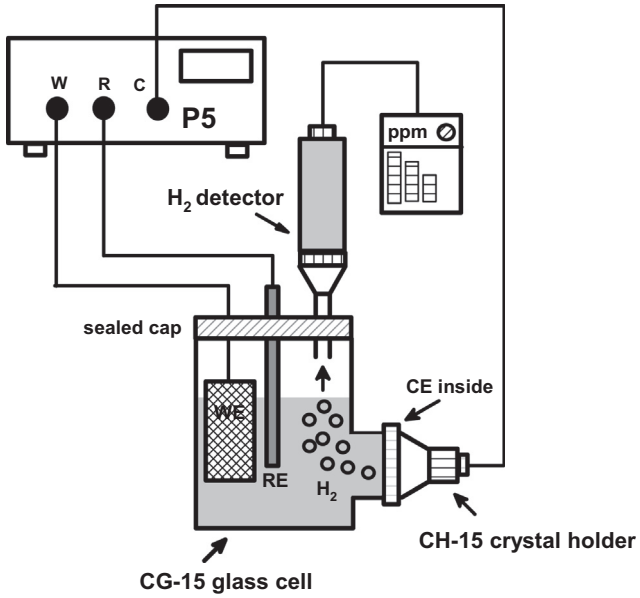

Scheme 4 Arrangement employed for studying H_2 evolution from a Pt-coated quartz crystal (CE) while urea contained in aqueous 0.1 M NaOH is electrolyzed on TiO_2-bearing (ITO/TiO_2//Ni^{II}cyclam) or non-TiO_2-bearing (ITO//Ni^{II}cyclam) anodes as working-electrodes (WE).

turbation from 1 MHz to 20 mHz (delay time = 30 s). To interpretate these analyses, an appropriate equivalent circuit was fitted to all the spectra with the aid of the SIM® Zahner-Elektrik software.

2.5. H_2O reduction on polycrystalline platinum

H_2O reduction was studied on a 3 mm diameter polycrystalline Pt disk (**WE**) using CV (see Scheme 3). The testing was performed by an Epsilon® BASi potentiostat-galvanostat (**P4**). Here, the potentiostat **P4** was connected to a typical three-electrode cell containing deoxygenated aqueous 0.1 M NaOH at 25 °C. To complete the electrical system, a Ag|AgCl 3 M NaCl reference electrode (**RE**) and a polycrystalline Pt wire-counter electrode (**CE**) were inserted into the cell.

2.6. Urea electrolysis and simultaneous H_2 generation

Urea electrolysis on **ITO/TiO_2//Ni^{II}cyclam** or **ITO//Ni^{II}-cyclam** anodes (as the **WE**), and H_2O reduction on Pt cathodes were simultaneously studied utilizing a 45-mL GC-15 Inficon glass cell (see Scheme 4) equipped with a 12.7 mm diameter

Please cite this article in press as: Murcio-Hernández, S. et al., Electrocatalytic urea mineralization in aqueous alkaline medium using Ni^{II}cyclam-modified nanoparticulate TiO_2 anodes and its relationship with the simultaneous electrogeneration of H_2 on Pt counterelectrodes. Arabian Journal of Chemistry (2018), https://doi.org/10.1016/j.arabjc.2017.12.029

polished Pt disk (as the **CE**) supported on a 149240-1 Maxtek AT-cut 25.4 mm diameter quartz crystal. Here, a Maxtek CHC-15 crystal holder was utilized to couple this cathode into the GC-15 cell. In this study, 30 mL of deoxygenated aqueous solution containing 0.1 M NaOH plus 10 mM urea was added to the cell. Either of the test **WE**, an Ag|AgCl 3 M NaCl (**RE**), and a HY-ALERTA H2scan® model 500 H_2 sensor probe with a specific leak detector, were also employed using a commercial 'sealed cap' adapted to the GC-15 cell.

Any H_2 gas that evolved from the Pt cathode (as suggested by Eq. (12)) was monitored *in situ* using the H_2 detector, while the urea electrolysis was carried out on either of the **WE** anodes by the controlled potential electrolysis (CPE) technique, performed using an Epsilon® BASi potentiostat-galvanostat (**P5**).

Here, the urea electrolysis (via Eq. (1)) was also monitored *ex situ* by measuring the total organic carbon (TOC) removal from the bulk electrolytic solution. TOC measurements were obtained with a V_{CSN}® Shimadzu TOC analyser equipped with an ASI-V sampler.

3. Results and discussion

3.1. Preparation of nanoparticulate TiO_2-coated ITO electrodes

The nanometric structure for electrophoretically deposited nanoparticulate TiO_2 films on ITO electrodes was confirmed by High-Resolution SEM (Fig. 1A).

A comparison between Fig. 1A and B presents the homogeneous surfaces of nanoparticulate TiO_2-modified ITO electrodes and bare ITO electrodes, respectively. Furthermore, a detailed comparison between the insets in each image clearly confirm the nanoporous morphology for the TiO_2 films (Fig. 1A-inset), and the flat surface of the ITO substrates (Fig. 1B-inset) in good agreement with a roughness factor of 1.3 (Yamada et al., 2003).

3.2. Preparation of Ni^{II}cyclam-modified nanoparticulate TiO_2-coated ITO anodes

Fig. 2 shows the evolution of the CV responses obtained for electroformation of Ni^{II}cyclam films on the ITO/TiO_2 (Fig. 2A-*ii*, system **ITO/TiO_2//Ni^{II}cyclam**, continuous lines) and ITO (Fig. 2B-*ii*, system **ITO//Ni^{II}cyclam**, continuous lines) electrodes immersed in a monomer solution of Ni^{II}-cyclam (Manriquez et al., 1999; Ferrer et al., 2003). Examining Fig. 2A-*ii* and 2B-*ii* one observes the continuous increase of the current peak intensity at 0.55 and 0.45 V, respectively, thus indicating that Ni^{II}cyclam-based films were growing on ITO/TiO_2 and ITO anodes due to the anodic oxidation of the Ni (II) cations localized at the Ni^{II}cyclam monomers (Bukowska et al., 1996; Alatorre-Ordaz et al., 1998).

A detailed analysis of Fig. 2A-*ii* and 2B-*ii* reveals that the CV peaks observed between scans 3 and 6 can be associated with the increment of the surface coverage of electroactive Ni^{II}cyclam monomers by development of oxo-bridges (**O-Ni^{III}-O**) between **Ni^{III} sites** (Supplementary Data SD-1, processes C and D) (Bukowska et al., 1996; Alatorre-Ordaz et al., 1998). However, this process is viable only when CV scans 1 and 2 show two irreversible voltammetric signals, which are linked to the electrochemical adsorption of Ni^{II}-

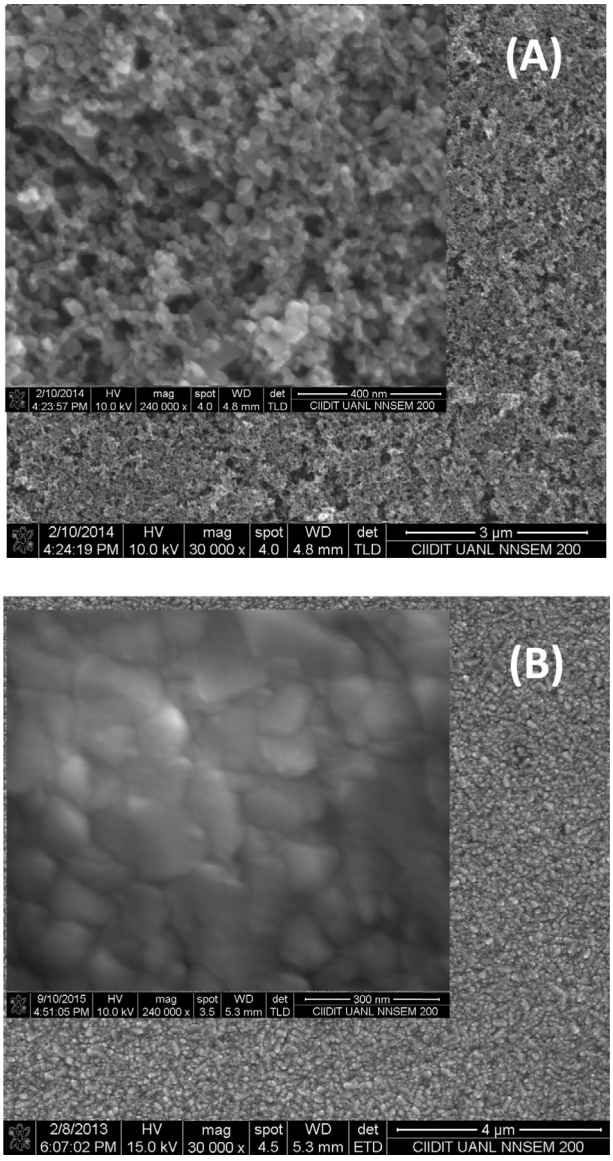

Fig. 1 High-resolution SEM images obtained for (A) nanoparticulate TiO_2-coated ITO electrodes and (B) naked ITO electrodes, magnification 30 kX and 240 kX (insets).

cyclam molecules on the electrode surface (Rosłonek and Taraszewska, 1992) via oxidation of cyclam moieties (Supplementary Data SD-1, processes A and B) (Pierozynski, 2013; Alatorre-Ordaz et al., 1998).

The apparent surface coverages of electroactive Ni^{II}cyclam monomers ($\Gamma_{Ni\text{-}cyclam}$) on the **ITO/$TiO_2$//$Ni^{II}$cyclam** and **ITO//$Ni^{II}$cyclam** electrodes were estimated by CV (Supplementary Data SD-4) as $(3.09 \pm 0.89)\times10^{-10}$ and $(9.71 \pm 0.12)\times10^{-8}$ mol cm^{-2}, respectively. The surface density of electropolimerized Ni^{III} sites on ITO electrodes was 314 higher than for ITO/TiO_2 electrodes. This observation strongly suggests that the large number of Ti-O^- groups contained on the ITO/TiO_2 electrodes act to reduce the entry of OH^- anions into the TiO_2 pores. Consequently, the O-Ni^{III}-O oxo-bridges insertions (Supplementary Data SD-1, processes C and D) would be less favourable on ITO/TiO_2 structure, producing the lower-coverage electropolymerized Ni^{II}cyclam films as

Please cite this article in press as: Murcio-Hernández, S. et al., Electrocatalytic urea mineralization in aqueous alkaline medium using Ni^{II}cyclam-modified nanoparticulate TiO_2 anodes and its relationship with the simultaneous electrogeneration of H_2 on Pt counterelectrodes. Arabian Journal of Chemistry (2018), https://doi.org/10.1016/j.arabjc.2017.12.029

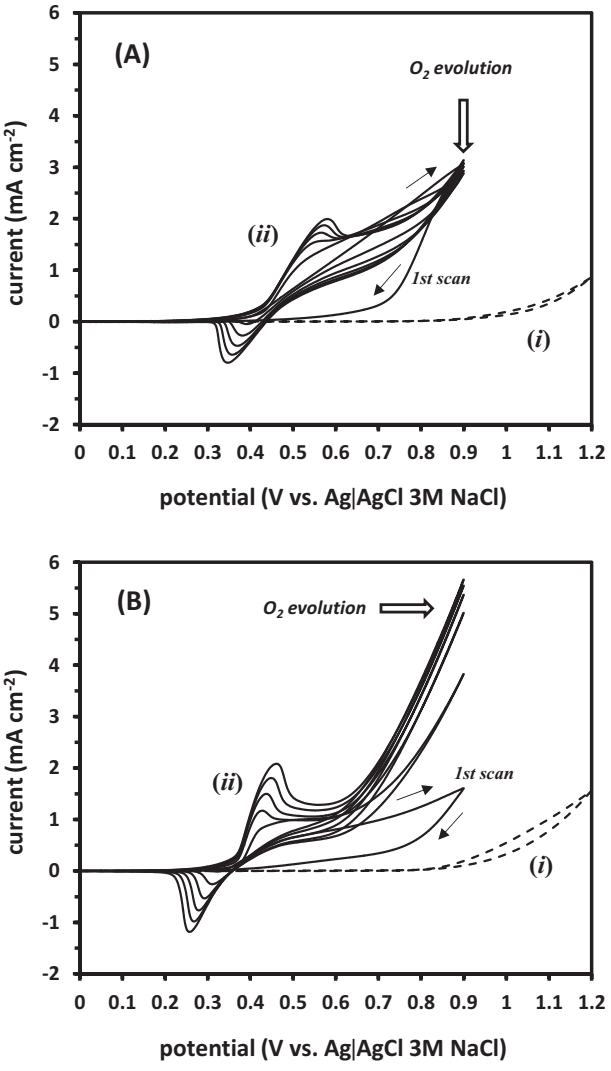

Fig. 2 Consecutive cyclic voltammograms obtained for the electroformation of Ni^{II}cyclam coatings on (A-*ii*) ITO/TiO_2 and (B-*ii*) ITO electrodes, both immersed in a deoxygenated aqueous 0.1 M NaOH plus 2 mM Ni^{II}cyclam solution (only 6 scans are shown for comparison purposes). CV responses for ITO/TiO_2 and ITO electrodes immersed in deoxygenated 0.1 M NaOH without monomers are shown in figures 2A-*i* and 2B-*i*, respectively. dE/dt = 25 mV s^{-1} in both cases.

confirmed by EDS elemental analysis (see Fig. 3A and Table SD-4 at the Supplementary Data SD-4) (Rosłonek and Taraszewska, 1994). Higher-coverage electropolymerized Ni^{II}-cyclam films were produced on the bare ITO electrodes as confirmed by EDS elemental analysis and shown in Fig. 3B and Table SD-4 of the Supplementary Data SD-4), apparently due to the excess of OH^- ions being transported to the ITO surface from the bulk electrolyte without the controlling behaviour of protective TiO_2 coatings.

To gain further insight, a new review of Fig. 2A-*ii* and B-*ii* revealed that the cogeneration of O_2 (via Eqs. (13)–(15), where L = cyclam) (Malinski et al., 1991; Liu et al., 2017) during the voltammetric preparation of **ITO/TiO_2//Ni^{II}cyclam** electrodes (Fig. 2A-*ii*) was significantly lower than during the voltammetric preparation of **ITO//Ni^{II}cyclam** electrodes (Fig. 2B-*ii*). These observations confirm that the reaction (Eq. (15)) must have been fed by a significantly lower number of OH^- anions (Eq. (13)) when ITO substrates were coated with TiO_2 films.

$$[O-Ni^{II}L\sim \mathbf{Ni^{III}(OH)}L-O]^{3+}+OH^- \rightarrow [O-Ni^{II}L\sim \mathbf{Ni^{IV}(OH)_2}L-O]^{3+}+e^- \quad (13)$$

$$[O-Ni^{II}L\sim \mathbf{Ni^{IV}(OH)_2}L-O]^{3+} \rightarrow [O-Ni^{II}L\sim (\mathbf{O=Ni^{IV}}L)-O]^{3+}+H_2O \quad (14)$$

$$[O-Ni^{II}L\sim (\mathbf{O=Ni^{IV}}L)-O]^{3+} \rightarrow [O-Ni^{II}L\sim Ni^{II}L-O]^{3+}+1/2\mathbf{O_2} \quad (15)$$

3.3. Electrocatalytic urea oxidation on ITO/TiO_2//Ni^{II}cyclam and ITO//Ni^{II}cyclam anodes

Electrocatalytic capabilities of the urea oxidation on **ITO/TiO_2//Ni^{II}cyclam** (Fig. 4A) and **ITO//Ni^{II}cyclam** (Fig. 4B) electrodes were explored in aqueous 0.1 M NaOH with cyclic voltammetry (CV) while employing Scheme 2B.

In an initial inspection of Fig. 4 one can recognize the typical shape of the voltammetric responses for urea oxidation on Ni^{II}cyclam-modified electrodes (Manriquez et al., 1999; Ferrer et al., 2003). This voltammetric behaviour is also comparable to those reported for methanol (Liu, 2004; Trevin et al., 1997), hydrazine (Trevin et al., 1997) and formaldehyde (Ciszewski and Miczarek, 1999) oxidation on Ni(II) macrocyclic-based films. Fig. 4 contains two anodic peaks associated with urea oxidation (**ap_2**) observed in the forward sweeps at 0.78 and 0.81 V on **ITO/TiO_2//Ni^{II}cyclam** (Fig. 4A) and **ITO//Ni^{II}cyclam** (Fig. 4B) electrodes, respectively. Particularly, in Fig. 4A the peak **ap_2** appears clearly paired with the signal assigned to the redox transition (Ni^{II} ⇄ Ni^{III})cyclam (**ap_1**, shoulder towards 0.57 V). However, in Fig. 4B the respective peak **ap_1** is not observed because this signal has been overlapped by the peak **ap_2**. Here the shape of the voltammetric responses, presented in Fig. 4, indicates that the electroadsorption of urea molecules on **Ni^{III} sites** (i.e. [O–Ni^{II}-L∼**Ni^{III}(OH)**L–O]$^{3+}$) localized at electroactivated **ITO/TiO_2//Ni^{II}cyclam** (Fig. 4A) and **ITO//Ni^{II}cyclam** (Fig. 4B) electrodes is thermodynamically favourable in both cases. Furthermore, the overlapping of peaks **ap1** and **ap2** in Fig. 4B strongly suggests that the bonding energy between urea molecules and [O–Ni^{II}L∼**Ni^{III}(OH)**L–O]$^{3+}$ sites in ITO//Ni^{II}-cyclam electrodes was higher than between urea molecules and the same sites in the ITO/TiO_2//Ni^{II}cyclam electrodes.

The reverse sweeps in Fig. 4A and B reveals two anodic peaks (**ap_3**) towards 0.72 and 0.61 V for ITO/TiO_2//Ni^{II}cyclam and ITO//Ni^{II}cyclam electrodes, respectively. These could be attributed to the oxidation of adsorbed intermediates (Guo et al., 2015; Chen et al., 2004; Huang et al., 2004; Gagné and Ingle, 1981). Particularly, it has been reported that during the forward sweep of the voltammetric urea oxidation, carbon monoxide C≡O intermediates can be adsorbed (**CO_{ads}**) on the electrocatalytic Ni^{III} sites localized at NiO(OH) films (Guo et al., 2015; Huang et al., 2004). Thereafter, when the surface density of absorbed intermediates [O–Ni^{II}L∼**Ni^{III}(OH)**L–O]$^{3+}$·(**CO_{ads}**) is relatively low, they can be oxidized to CO_2 during the voltammetric reverse sweep to release the **Ni^{II} centers** (i.e.

Please cite this article in press as: Murcio-Hernández, S. et al., Electrocatalytic urea mineralization in aqueous alkaline medium using Ni^{II}cyclam-modified nanoparticulate TiO_2 anodes and its relationship with the simultaneous electrogeneration of H_2 on Pt counterelectrodes. Arabian Journal of Chemistry (2018), https://doi.org/10.1016/j.arabjc.2017.12.029

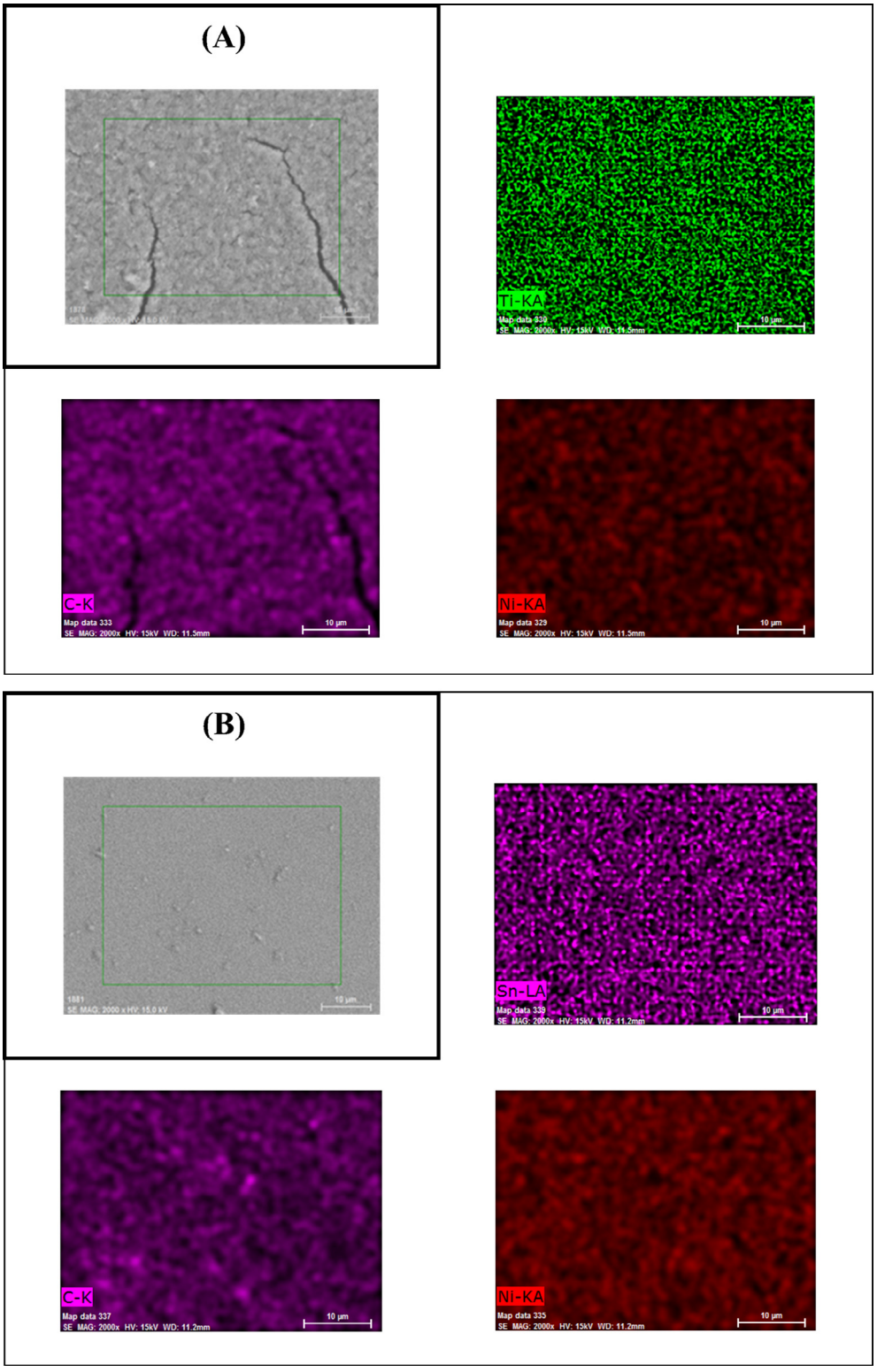

Fig. 3 SEM images obtained at the outer face of (A) TiO_2-bearing anodes (system ITO/TiO_2//Ni^{II}cyclam) and (B) non-TiO_2-bearing anodes (system ITO//Ni^{II}cyclam). Insets: Comparative mappings of key elements obtained by EDS analysis into the green frameworks as follows: (A) K-lines of Ti, C and Ni for the TiO_2|Ni^{II}cyclam junction and, (B) K-lines of Sn, In, C and Ni for the ITO|Ni^{II}cyclam junction. Magnifications of 2 kX and accelerating voltages of 15 kV were employed in all the cases.

$[O–Ni^{II}L\sim Ni^{II}L–O]^{3+}$) via Eq. (16) (Huang et al., 2004). On the other hand, when the surface density of $[O–Ni^{II}L\sim$**Ni^{III}(OH)**$L–O]^{3+}\cdot$**(CO_{ads})** units is very high, the inactivation of $[O–Ni^{II}L\sim Ni^{II}L–O]^{3+}$ centers is caused by formation of chemically stable $[O–$**($Ni^{I}CO$)**$L\sim$**($Ni^{I}CO$)**$L–O]^{3+}$ monocarbonyl complexes (Eq. (17)). Here $K_{CO} > 10^2\ M^{-1}$ is the

Please cite this article in press as: Murcio-Hernández, S. et al., Electrocatalytic urea mineralization in aqueous alkaline medium using Ni^{II}cyclam-modified nanoparticulate TiO_2 anodes and its relationship with the simultaneous electrogeneration of H_2 on Pt counterelectrodes. Arabian Journal of Chemistry (2018), https://doi.org/10.1016/j.arabjc.2017.12.029

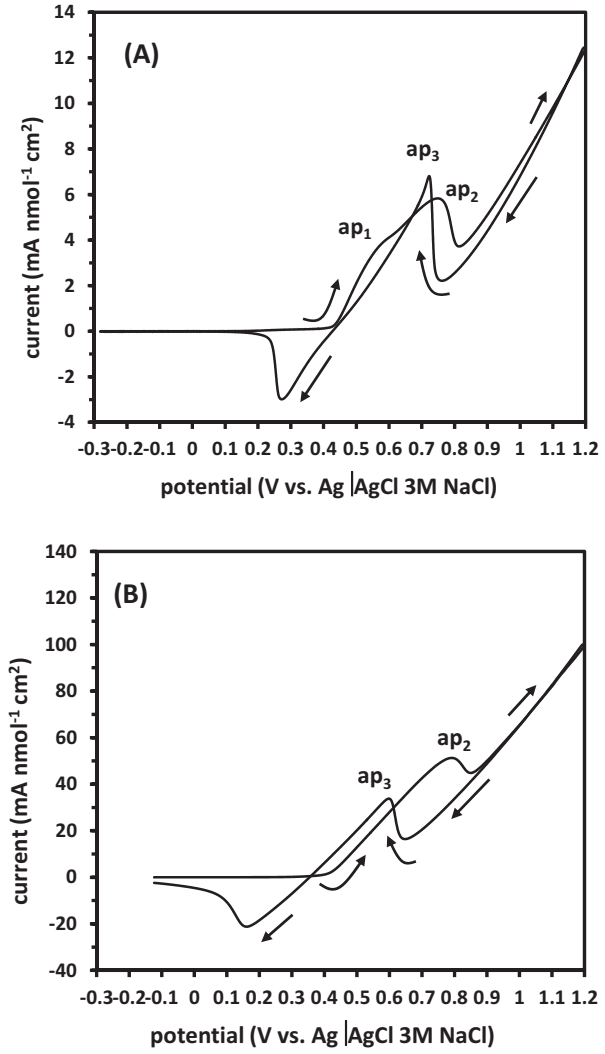

Fig. 4 Cyclic voltammograms obtained for the oxidation of urea on (A) TiO_2-bearing anodes (ITO/TiO_2//Ni^{II}cyclam) and (B) non-TiO_2-bearing anodes (ITO//Ni^{II}cyclam) immersed in deoxygenated aqueous 0.1 M NaOH plus 10 mM urea. Currents were normalized regarding the respective values of $\Gamma_{Ni\text{-}cyclam}$ (Section 3.2), while dE/dt = 25 mV s^{-1} in both cases.

equilibrium binding constant between nickel complexes and **CO** intermediates (Gagné and Ingle, 1981). To gain insight into the $\mathbf{CO_{ads}}$ oxidation during the reverse sweeps in Fig. 4A and B, a comparison between the $\mathbf{CO_{ads}}$ oxidation potentials ($\mathbf{E_{ap3}}$) in these figures was performed. This analysis strongly suggests that the oxidation of these intermediates is favored in the presence of nanoparticulate TiO_2 films via Eq. (16). This was inferred because $\mathbf{E_{ap3}}$ in the system ITO/TiO_2//Ni^{II}cyclam (0.72 V, Fig. 4A) was shifted positively compared to the system ITO//Ni^{II}cyclam (0.61 V, Fig. 4B) (Huang et al., 2004). This last observations strongly suggests that the oxophilicity of Ni(III) cations at $[O\text{–}Ni^{II}L\sim\mathbf{Ni^{III}(OH)}L\text{–}O]^{3+}$ sites is strongly reduced in the presence of nanoparticulate TiO_2 surfaces, thus favoring the oxygen transfer towards $\mathbf{CO_{ads}}$ molecules.

$$[O - Ni^{II}L \sim \mathbf{Ni^{III}(OH)}L - O]^{3+} \cdot (\mathbf{CO_{ads}}) \rightarrow [O - Ni^{II}L \sim Ni^{II}L - O]^{3+} + \mathbf{CO_2} + H_2O \quad (16)$$

$$[O - Ni^{II}L \sim Ni^{II}L - O]^{3+} + \mathbf{2CO} \rightleftarrows [O - (\mathbf{Ni^{I}CO})L \sim (\mathbf{Ni^{I}CO})L - O]^{3+} \quad K_{CO} > 10^2\ M^{-1} \quad (17)$$

New comparisons between $\mathbf{j_{ap2}}$ (urea oxidation current at **ap2**) and $\mathbf{j_{ap3}}$ ($\mathbf{CO_{ads}}$ oxidation current at **ap3**) in Fig. 4A and B were carried out to better support this reasoning. These comparisons revealed that for **ITO/TiO_2//Ni^{II}-cyclam** electrodes the ratio j_{ap3}/j_{ap2} was approximately 1.1 (Fig. 4A) while it was about 0.6 for ITO//Ni^{II}cyclam electrodes (Fig. 4B). These values indicate that with TiO_2 nanoparticles (Fig. 4A), all the electrocatalytic $[O\text{–}Ni^{II}L\sim\mathbf{Ni^{III}(OH)}L\text{–}O]^{3+}$ sites which were employed by the urea oxidation reaction (Eq. (11)) during the forward sweep, were available during the reverse sweep for completing the oxidation of the $\mathbf{CO_{ads}}$ intermediates via Eq. (16). In contrast, in the absence of TiO_2 nanoparticles (Fig. 4B), more than the half of the $[O\text{–}Ni^{II}L\sim Ni^{II}L\text{–}O]^{3+}$ centers were blocked during the forward sweep with an excess of **CO** intermediates to produce $[O\text{–}(\mathbf{Ni^{I}CO})L\sim(\mathbf{Ni^{I}CO})L\text{–}O]^{3+}$ species via Eq. (17).

3.4. H_2O reduction on polycrystalline platinum

After the urea oxidation reaction was studied on working electrodes, the H_2O reduction reaction was studied on the Pt electrode while employing the Scheme 3 with aqueous 0.1 M NaOH as the electrolyte. The information obtained from this experiment was available to couple both anodic and cathodic processes using the cell design shown in Scheme 1.

Cyclic voltammograms for H_2O reduction are presented in Fig. 5. An inspection of Fig. 5A demonstrates that H_2 evolution is activated starting at −1.0 V, while a review of Fig. 5B

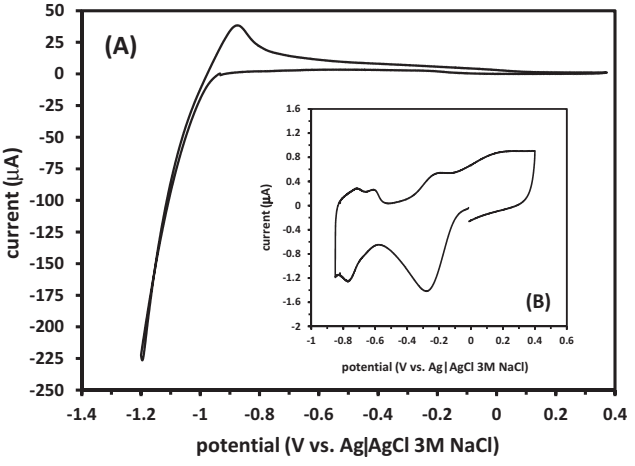

Fig. 5 Cyclic voltammogram obtained for H_2O reduction on a polycrystalline Pt electrode immersed in deoxygenated aqueous 0.1 M NaOH where cathodic limits were (A) −1.2 and (B) −0.9 V vs. RE. In both cases dE/dt = 25 mV s^{-1}.

Please cite this article in press as: Murcio-Hernández, S. et al., Electrocatalytic urea mineralization in aqueous alkaline medium using Ni^{II}cyclam-modified nanoparticulate TiO_2 anodes and its relationship with the simultaneous electrogeneration of H_2 on Pt counterelectrodes. Arabian Journal of Chemistry (2018), https://doi.org/10.1016/j.arabjc.2017.12.029

(inset) reveals the voltammetric signals for the H adsorption process begins between −0.6 and −0.9 V (Sheng and Gasteiger, 2010; Daubinger et al., 2014). These results suggest that H_2 evolution could be promoted on the Pt cathode if sufficient electrons were produced by the urea oxidation on either the **ITO/TiO$_2$//Ni^{II}cyclam** or **ITO//Ni^{II}cyclam** anodes to overcome a cathodic potential of −1.0 V vs. **RE**.

3.5. Coupling the electrocatalytic urea electrolysis with H_2O reduction for promoting H_2 evolution

CA experiments were conducted following Scheme 2A to coupling the electrocatalytic urea electrolysis on either the **ITO/TiO$_2$//Ni^{II}cyclam** or **ITO//Ni^{II}cyclam** anodes and H_2O reduction on a Pt cathode. Here, the Ni^{II}cyclam-modified anodes and the Pt cathode were immersed in a deoxygenated aqueous solution containing 0.1 M NaOH plus 10 mM urea at 25 °C. A set of single anodic potential steps were applied for 60 s to both Ni^{II}cyclam-modified electrodes to simultaneously record a set of the current-time responses generated from either the polarized **ITO/TiO$_2$//Ni^{II}cyclam** (Fig. 6A) or the **ITO//Ni^{II}-cyclam** (Fig. 6B) anodes at 0.4, 0.5, 0.6, 0.7, 0.8, 0.9, 1.0 and 1.1 V vs. **RE1**, and the respective set of potential vs. **RE2** – time responses at the Pt cathode (Fig. 6A-*inset* or Fig. 6B-*inset*, respectively).

Comparing between the insets demonstrates that the Pt cathode achieved a steady-state potential of −1.0 V vs. **RE2** when the TiO_2-bearing anode was polarized at +0.8 V vs. **RE1**. Contrastly, the non-TiO_2-bearing anode, allowed the Pt cathode to achieve a steady-state potential of −1.0 V vs. **RE2** only when the anode was polarized at +1.0 V vs. **RE1**. It is reasonable to surmise that this difference of 0.2 V is equivalent to the energetic difference between the potential peaks associated with CO oxidation (**ap3**) on the TiO_2-bearing and non-TiO_2-bearing anodes (review Fig. 4A and B, respectively). Consequently, it is clear that another effect of the TiO_2 nanoparticles on the electrocatalytic behaviour of the [O–Ni^{II}-L∼**Ni^{III}(OH)**L–O]$^{3+}$ sites should correspond to an effective charge separation on the semiconducting ITO|TiO_2 junction (see Scheme 5 for more details).

Considering Eq. (12), and viewing Fig. 5, the combination between a cathodic potential of −1.0 V vs. **RE2** (Fig. 6A-*inset*) and a steady-state urea electrolysis current of about 1.0 mA on an **ITO/TiO$_2$//Ni^{II}cyclam** anode, polarized at +0.8 V vs. **RE1** (see Fig. 6A beyond 40 s), was enough to activate progressive H_2 evolution from the Pt counter-electrode (Fig. 7-*i*, window time = 10 s). By contrast, an instantaneous activation of the H_2 evolution from the Pt cathode (Fig. 7-*ii*, window time = 10 s) polarized at the −1.0 V vs. **RE2** (Fig. 6A-*inset*), was achieved when an **ITO//Ni^{II}cyclam** anode was polarized at +1.0 V vs. **RE1** which established a steady-state urea electrolysis current of about 0.2 mA (see Fig. 6B beyond 40 s).

At first glance, these observations strongly suggest that the activation kinetics of the urea oxidation reaction would be faster on non-TiO_2-bearing electrodes (**ITO//Ni^{II}cyclam**) than on TiO_2-bearing electrodes (**ITO/TiO$_2$//Ni^{II}cyclam**), because the apparent surface coverage of Ni^{II}cyclam monomers ($\Gamma_{Ni\text{-}cyclam}$) on **ITO//Ni^{II}cyclam** electrodes is higher than on **ITO/TiO$_2$//Ni^{II}cyclam** electrodes (see Section 3.2). However, the alternating profile of the H_2 evolution in Fig. 7-*i* (beyond 30 min) supports the viability of the Eq. (16). Consequently, it

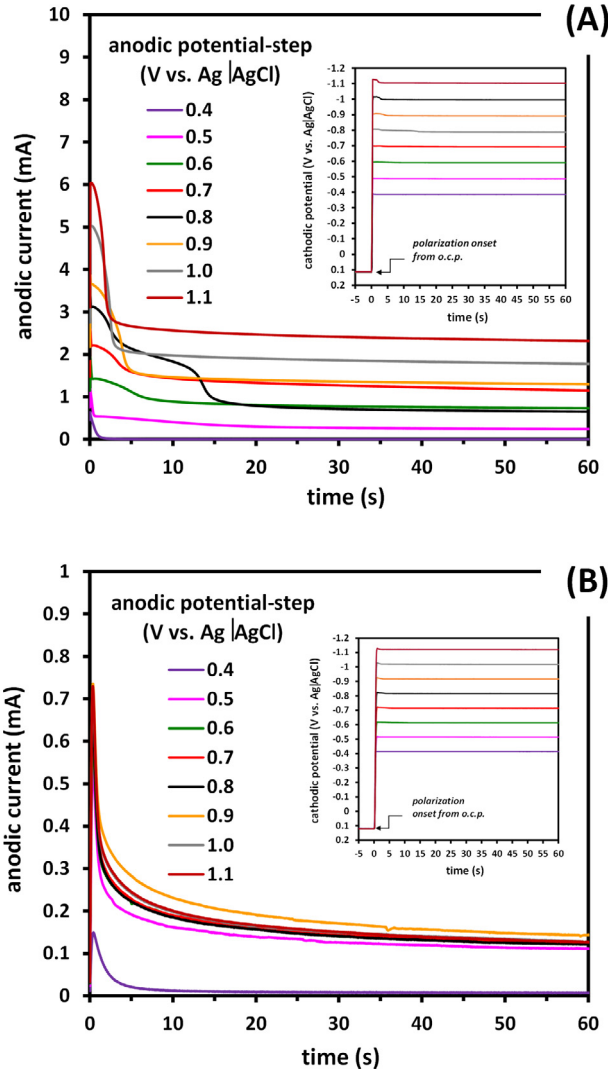

Fig. 6 Set of current-time responses generated from polarized (A) TiO_2-bearing anodes (ITO/TiO_2//Ni^{II}cyclam) and (B) non-TiO_2-bearing anodes (ITO//Ni^{II}cyclam) at 0.4, 0.5, 0.6, 0.7, 0.8, 0.9, 1.0 and 1.1 V vs. RE1, both immersed in a deoxygenated solution of aqueous 0.1 M NaOH plus 10 mM urea at 25 °C. Insets: Set of potential vs. RE2-time responses generated from a Pt cathodes during the polarization of the ITO/TiO_2//Ni^{II}cyclam (A) and ITO//Ni^{II}cyclam (B) anodes.

would be expected that the H_2 evolution efficiency would decrease when the urea oxidation on the available [O–Ni^{II}-L∼**Ni^{III}(OH)**L–O]$^{3+}$ sites promote the formation of [O–Ni^{II}-L∼**Ni^{III}(OH)**L–O]$^{3+}$·(**CO$_{ads}$**) intermediates, but then increase again if the adsorbed C≡O molecules (**CO$_{ads}$**) are oxidized to CO_2 which occurs more readily with the presence of the TiO_2 nanoparticles.

3.6. Activation kinetics of urea oxidation on ITO/TiO_2// Ni^{II}cyclam and ITO//Ni^{II}cyclam anodes

To better understand the activation kinetics of urea oxidation, EIS spectra were obtained using the arrangement called Scheme 2B where ITO/TiO_2//Ni^{II}cyclam (Fig. 8A, circles)

Please cite this article in press as: Murcio-Hernández, S. et al., Electrocatalytic urea mineralization in aqueous alkaline medium using Ni^{II}cyclam-modified nanoparticulate TiO_2 anodes and its relationship with the simultaneous electrogeneration of H_2 on Pt counterelectrodes. Arabian Journal of Chemistry (2018), https://doi.org/10.1016/j.arabjc.2017.12.029

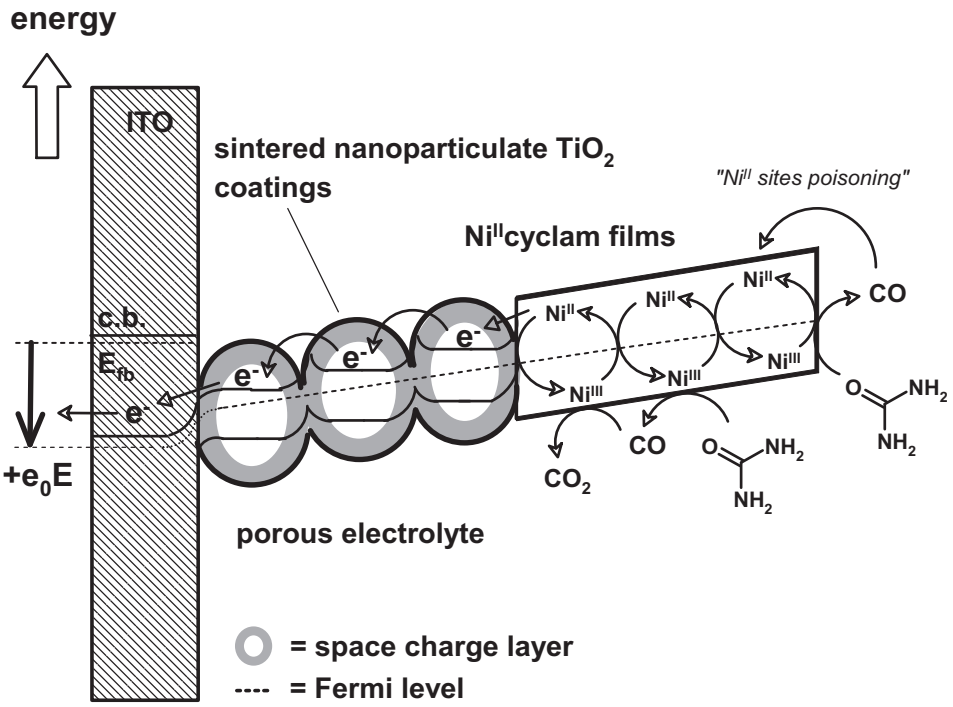

Scheme 5 Representation of the electrocatalytic urea oxidation on $[O–Ni^{II}L\sim\mathbf{Ni^{III}(OH)}L–O]^{3+}$ sites existing into TiO_2-bearing anodes ($ITO/TiO_2//Ni^{II}$cyclam), the effective charge separation on the semiconducting $ITO|TiO_2$ junction and the $[O–Ni^{II}L\sim Ni^{II}L–O]^{3+}$ centers poisoned by CO molecules. E and E_{fb} represent the applied interfacial potential and the ITO flatband potential, respectively. Finally, *c.b.* and e_o stand for the ITO conduction band and the fundamental charge, respectively.

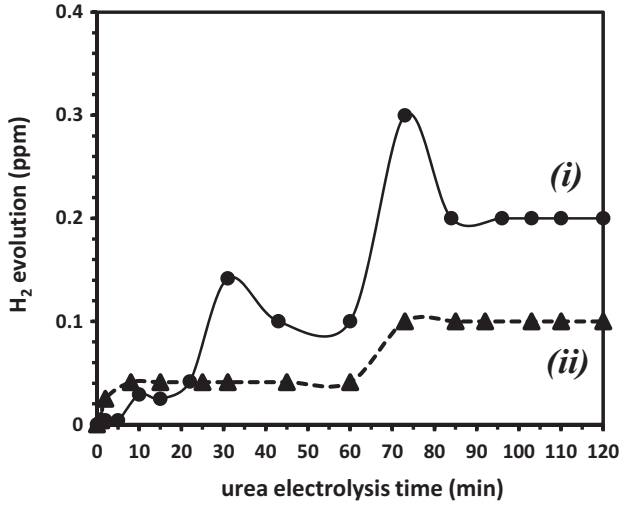

Fig. 7 Profiles of H_2 evolution rate from Pt cathodes during the anodic urea electrolysis performed on polarized (*i*) TiO_2-bearing anodes ($ITO/TiO_2//Ni^{II}$cyclam) or (*ii*) non-TiO_2-bearing anodes ($ITO//Ni^{II}$cyclam) at 0.8 V vs. RE, both immersed in a deoxygenated solution of aqueous 0.1 M NaOH plus 10 mM urea at 25 °C (see Scheme 4 for details about the experimental arrangement). Contribution of H_2 produced by anodic conversion of H_2O to O_2 (Eqs. (13)–(15)) was previously subtracted from all the experimental data using electrolysis in the absence of urea.

and $ITO//Ni^{II}$cyclam (Fig. 9A, circles) anodes were polarized at 0.4 (*i*), 0.5 (*ii*), 0.6 (*iii*), 0.7 (*iv*), 0.8 (*v*), 0.9 (*vi*), 1.0 (*vii*) and 1.1 V (*viii*) vs. **RE1**. Herein, the equivalent circuits described in Figs. 8B and 9B were fitted (lines) to the EIS spectra shown in Figs. 8A and 9A, respectively.

The best-fitted electrical elements are compiled in Supplementary Data SD-6. In both equivalent circuits, the Gerischer element (Z_G) represents the series impedance $W_H = (R_s/C_p)^{1/2}$ per unit length (l) of a Ni^{II}cyclam film, where $R_s = (r_{s,i} + r_{s,e}) \times l$ is the combined electronic ($r_{s,i} \times l$) and ionic transport ($r_{s,e} \times l$) resistance associated with the ($Ni^{II} \rightleftarrows Ni^{III}$)cyclam transitions, while $C_p = c_p \times l$ is the capacitance associated with the urea adsorption onto the electrocatalytic films. The parameter $k_r = (R_p \times C_p)^{-1}$ is the effective reaction rate for the electrocatalytic oxidation of urea molecules previously adsorbed on the $[O–Ni^{II}L\sim\mathbf{Ni^{III}(OH)}L–O]^{3+}$ sites (under the assumption that the concentration of the reaction product can be considered constant), where $R_p = r_p \times l^{-1}$ represents the respective charge transfer resistance (Boukamp and Bouwmeester, 2003; Boukamp et al., 2006). Additionally, the elements C_{ads} and R_{ads} stand for the capacitance and the electron transfer resistance associated with the C≡O adsorption ($\mathbf{CO_{ads}}$) and its oxidative desorption as CO_2 (Eq. (16)), respectively. Thus the parameter $\tau_{Ni} = |R_{ads}| \times C_{ads}$ is the effective lifetime for the $[O–Ni^{II}L\sim\mathbf{Ni^{III}(OH)}L–O]^{3+}\cdot(\mathbf{CO_{ads}})$ intermediates before the $[O–Ni^{II}L\sim Ni^{II}L–O]^{3+}$ centers being irreversibly blocked by C≡O molecules (Eq. (17)) (Gagné and Ingle, 1981).

The element R_t represents the existing electrical resistances on the $ITO|TiO_2$ (Fig. 8B, where $R_t = R_{sol} + R_{ITO} + R_{junction} + R_{TiO2}$) or ITO (Fig. 9B, where $R_t = R_{sol} + R_{ITO}$) substrates. Here, R_{sol}, R_{ITO}, $R_{junction}$ y R_{TiO2} stand for the electrical resistances through the bulk electrolyte, the ITO surface, the ITO/TiO_2 junction and the nanoporous TiO_2 film. The element C_{ITO}, which appears in Fig. 8B, corresponds to the zones

Please cite this article in press as: Murcio-Hernández, S. et al., Electrocatalytic urea mineralization in aqueous alkaline medium using Ni^{II}cyclam-modified nanoparticulate TiO_2 anodes and its relationship with the simultaneous electrogeneration of H_2 on Pt counterelectrodes. Arabian Journal of Chemistry (2018), https://doi.org/10.1016/j.arabjc.2017.12.029

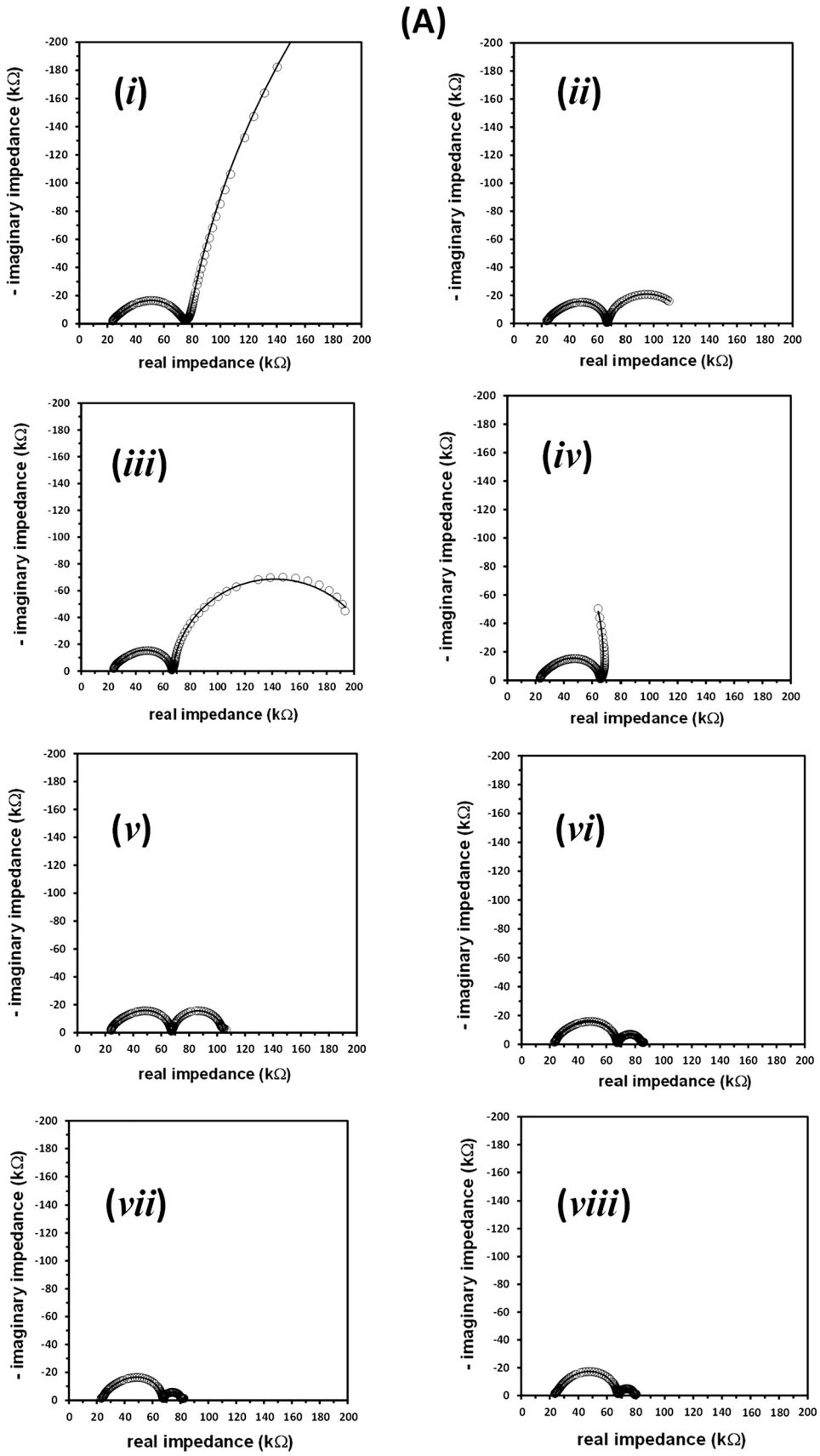

Fig. 8 (A) Circles are the experimental EIS spectra obtained for polarized TiO_2-bearing anodes (ITO/TiO_2//Ni^{II}cyclam) at 0.4 (*i*), 0.5 (*ii*), 0.6 (*iii*), 0.7 (*iv*), 0.8 (*v*), 0.9 (*vi*), 1.0 (*vii*) and 1.1 V (*viii*) vs. RE1, immersed in a deoxygenated solution of aqueous 0.1 M NaOH plus 10 mM urea at 25 °C. Solid lines corresponds to the best fitting of the equivalent circuit displayed in (B) to the experimental spectra.

Please cite this article in press as: Murcio-Hernández, S. et al., Electrocatalytic urea mineralization in aqueous alkaline medium using Ni^{II}cyclam-modified nanoparticulate TiO_2 anodes and its relationship with the simultaneous electrogeneration of H_2 on Pt counterelectrodes. Arabian Journal of Chemistry (2018), https://doi.org/10.1016/j.arabjc.2017.12.029

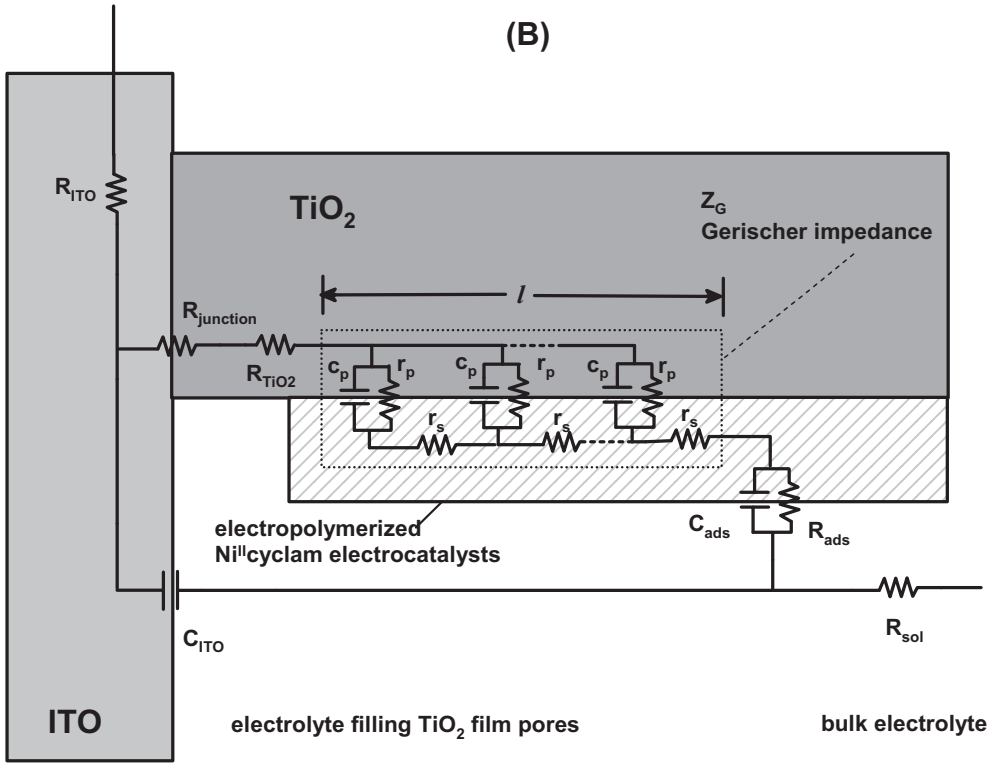

Fig. 8 (*continued*)

on the ITO surfaces which were not electrophoretically coated by TiO_2 nanoparticles and consequently, could reasonably be assumed that these zones do not show electrocatalytic activity while the EIS experiments were performed.

A first comparison between the spectra obtained for the electrocatalytic urea oxidation on **ITO/TiO$_2$//Ni^{II}cyclam** (Fig. 8A) and **ITO//Ni^{II}cyclam** (Fig. 9A) anodes, reveals that the oxidation of **CO$_{ads}$** to CO_2 (see all the low frequency couplings in Figs. 8A and 9A) is the rate determining step (r.d.s.) after the urea oxidation has been activated on both polarized electrodes (see all the high frequency couplings in Figs. 8A and 9A) when applying interfacial potentials higher than 0.4 V vs. **RE1** (see Fig. 4). Furthermore, the shape adopted by the low frequency responses of the spectra performed at 0.7 V vs. **RE1** (Figs. 8A-*iv* and 9A-*iv*) demonstrates that the formation of $[O–Ni^{II}L\sim\mathbf{Ni^{III}(OH)}L–O]^{3+}\cdot(\mathbf{CO_{ads}})$ intermediates becomes reversible when this energetic barrier is overcome to activate the Eq. (16).

Fig. 10 suggests that when the $[O–Ni^{II}L\sim\mathbf{Ni^{III}(OH)}L–O]^{3+}$ sites have been activated by interfacial potentials beyond 0.5 V vs. **RE1**, the effective urea oxidation rate (k_r) on **ITO//Ni^{II}-cyclam** electrodes was about 10^2 times higher than for **ITO/TiO$_2$//Ni^{II}cyclam** electrodes. These results confirmed that the urea oxidation rates on $[O–Ni^{II}L\sim\mathbf{Ni^{III}(OH)}L–O]^{3+}$ sites are strongly dependent from the apparent surface coverages ($\Gamma_{Ni\text{-}cyclam}$) of Ni^{II}cyclam. However, Fig. 11 reveals that when the interfacial potential exceeds 0.6 V vs. **RE1**, the effective lifetimes for the $[O–Ni^{II}L\sim\mathbf{Ni^{III}(OH)}L–O]^{3+}\cdot(\mathbf{CO_{ads}})$ intermediates (τ_{Ni}) on the polarized **ITO/TiO$_2$//Ni^{II}cyclam** electrodes were significantly longer than for those intermediates localized in the polarized **ITO//Ni^{II}cyclam** electrodes. This result strongly indicates that $[O–Ni^{II}L\sim Ni^{II}L–O]^{3+}$ centers poisoning by CO molecules (Eq. (17)) could be strongly inhibited in the presence of polarized TiO_2 nanoparticles (Scheme 5). Consequently, it is expected that the process of regeneration of electrocatalytic $[O–Ni^{II}L\sim\mathbf{Ni^{III}(OH)}L–O]^{3+}$ sites (Eqs. (8)–(10)) will immediately follow when the CO conversion to CO_2 via Eq. (16) occurs. This behaviour would improve the efficiencies of anodic urea mineralization (Eq. (11)) and of cathodic evolution of H_2 (Eq. (12)) in a single operating cell (Scheme 1).

The plausible explanation about the enhancement of **CO$_{ads}$** conversion to CO_2 during the urea oxidation on **ITO/TiO$_2$//Ni^{II}cyclam** anodes, seems related the adsorption of CO molecules on positive anatase TiO_2 surfaces adopting a preferential O≡C···Ti configuration at an adsorption energy of 0.45 eV (see Scheme 6) (Wanbayor et al., 2011). This adsorption energy is significantly stronger than for the O≡C···Ti configuration on neutral anatase TiO_2 (0.26 eV) (Wanbayor et al., 2011) and neutral rutile SnO_2 (0.25 eV) (Melle-Franco and Pacchioni, 2000), but it is comparable to neutral rutile TiO_2 (0.48 eV) (Sorescu and Yates, 1998). It is reasonable therefore, to assume that a polarized coating of sintered P25® TiO_2 nanoparticles, made up of 76% anatase and 24% rutile (Pérez-Viramontes et al., 2014; Kozuka et al., 2000), can adsorb and retain the CO molecules produced during the urea oxidation and inhibit the poisoning of $[O–Ni^{II}L\sim Ni^{II}L–O]^{3+}$ centers (Eq. (17)) thus aiding the regeneration of electrocatalytic $[O–Ni^{II}L\sim\mathbf{Ni^{III}(OH)}L–O]^{3+}$ sites (Eqs. (8)–(10)).

A more detailed review of Fig. 11 demonstrates that under low interfacial polarization (potentials between 0.4 and 0.6 V vs. **RE1**) the values of τ_{Ni} for **ITO/TiO$_2$//Ni^{II}cyclam** and **ITO//Ni^{II}cyclam** electrodes are comparable. However, under high interfacial polarization (potentials between 0.7 and 1.1

Please cite this article in press as: Murcio-Hernández, S. et al., Electrocatalytic urea mineralization in aqueous alkaline medium using Ni^{II}cyclam-modified nanoparticulate TiO_2 anodes and its relationship with the simultaneous electrogeneration of H_2 on Pt counterelectrodes. Arabian Journal of Chemistry (2018), https://doi.org/10.1016/j.arabjc.2017.12.029

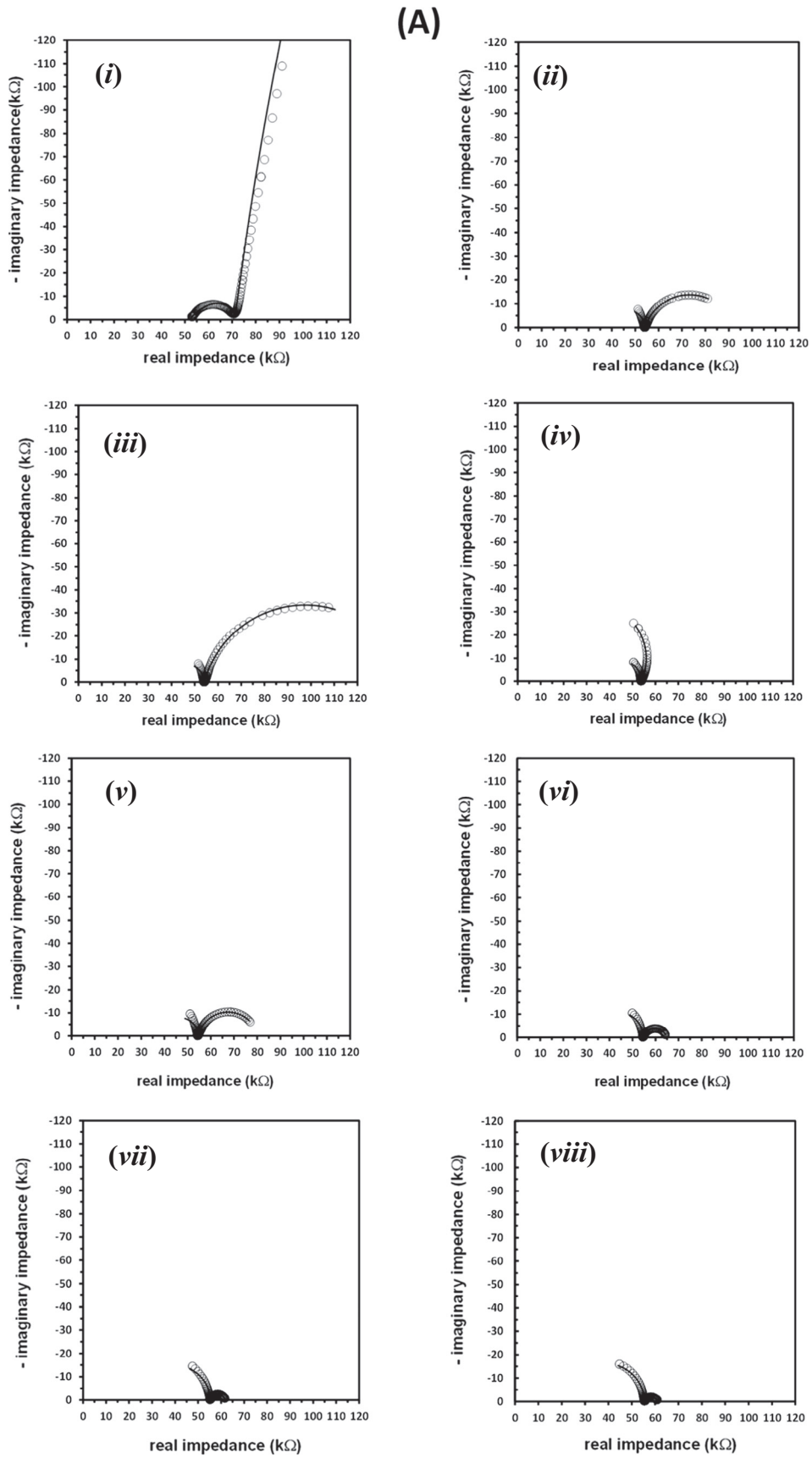

Fig. 9 (A) Circles are the experimental EIS spectra obtained for polarized non-TiO_2-bearing anodes (ITO//Ni^{II}cyclam) at 0.4 (*i*), 0.5 (*ii*), 0.6 (*iii*), 0.7 (*iv*), 0.8 (*v*), 0.9 (*vi*), 1.0 (*vii*) and 1.1 V (*viii*) vs. RE1, immersed in a deoxygenated solution of aqueous 0.1 M NaOH plus 10 mM urea at 25 °C. Solid lines corresponds to the best fitting of the equivalent circuit displayed in (B) to the experimental spectra.

Please cite this article in press as: Murcio-Hernández, S. et al., Electrocatalytic urea mineralization in aqueous alkaline medium using Ni^{II}cyclam-modified nanoparticulate TiO_2 anodes and its relationship with the simultaneous electrogeneration of H_2 on Pt counterelectrodes. Arabian Journal of Chemistry (2018), https://doi.org/10.1016/j.arabjc.2017.12.029

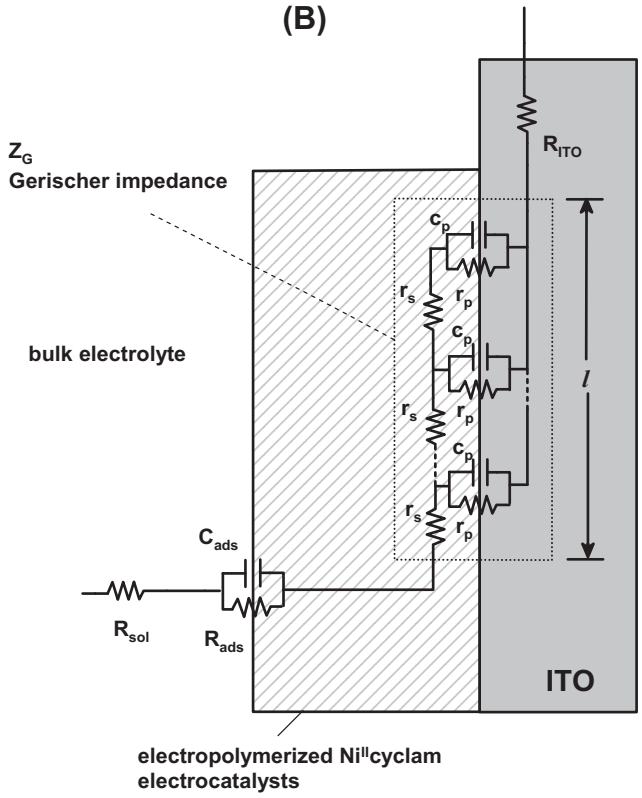

Fig. 9 (*continued*)

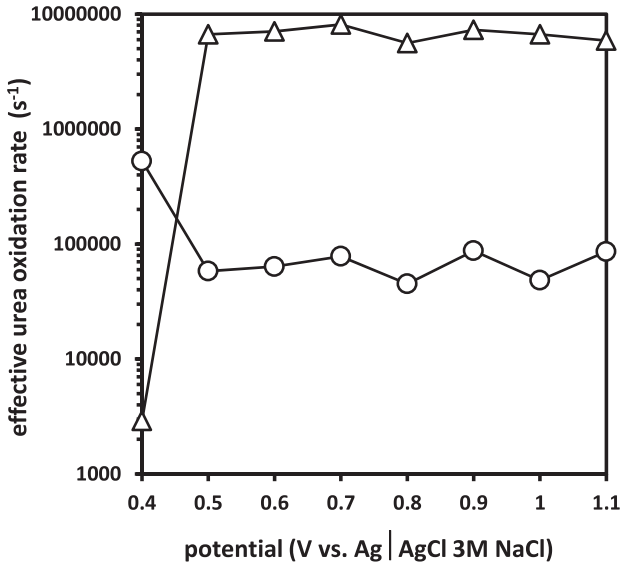

Fig. 10 Semi-logarithmic dependence of the effective urea oxidation rate (k_r) with the interfacial potentials which were applied to the (—O—) TiO_2-bearing anodes (ITO/TiO_2//Ni^{II}-cyclam) or (—Δ—) non-TiO_2-bearing anodes (ITO//Ni^{II}cyclam) during the urea oxidation.

V vs. **RE1**) the values of τ_{Ni} for the TiO_2-bearing anodes is higher than for the non-TiO_2-bearing anodes, confirming that the TiO_2 coatings have been activated for capturing CO molecules at these higher potentials.

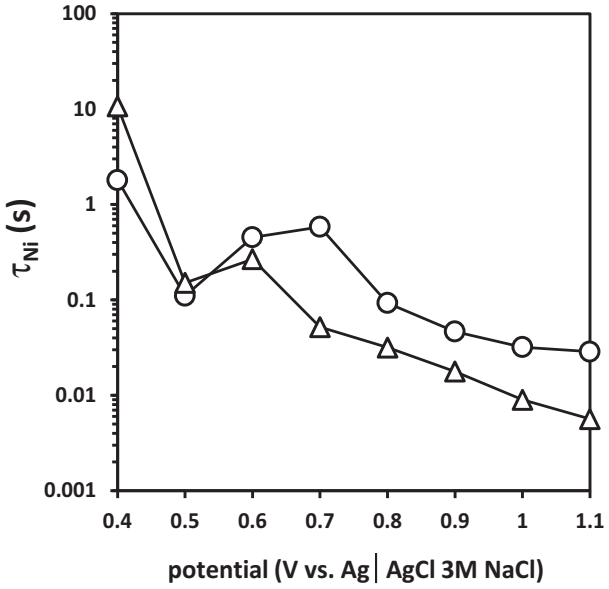

Fig. 11 Semi-logarithmic dependence of the effective lifetime of the $[O–Ni^{II}L\sim Ni^{III}(OH)L–O]^{3+}\cdot(CO_{ads})$ intermediates (τ_{Ni}) regarding the interfacial potentials which were applied to the (—O—) TiO_2-bearing anodes (ITO/TiO_2//Ni^{II}cyclam) or (—Δ—) non-TiO_2-bearing anodes (ITO//Ni^{II}cyclam) during the urea oxidation.

Further explanation for the CO capture phenomenon by TiO_2-bearing anodes (Fig. 6A) can be formulated by comparing the semiconductor properties of nanoparticulate ITO|TiO_2 and naked ITO electrodes. A comparison between the magnitudes of the reported donors concentration (N_D) for ITO/TiO_2 (10^{17}–10^{20} cm^{-3}) (Manríquez and Godínez, 2007; Heimer et al., 1994; Cao et al., 1980; Fabregat-Santiago et al., 2003) and ITO ($>10^{21}$ cm^{-3}) (Hassanzadeh et al., 2004; Turrión et al., 2003) electrodes, clearly indicates that the electronic charge separated by ITO/TiO_2 junctions is higher than for naked ITO electrodes. Therefore, it is reasonable to believe that the electrophoretically prepared ITO/P25® TiO_2 junctions containing a high concentration of Ti^{3+} donor sites (Manríquez and Godínez, 2007; Acevedo-Peña et al., 2010) improve the polarization of the C≡O molecular orbitals by π back-donation from the metal to the molecule (Wanbayor et al., 2011; Lustemberg and Scherlis, 2013), thus increasing the adsorption energy of the $O{\equiv}C\cdots Ti^{3+}$ configuration (0.45 eV for rutile and 0.96 eV for anatase (Lustemberg and Scherlis, 2013) during the urea oxidation on polarized TiO_2-bearing anodes (Zhang and Yates, 2010).

Based on this observation, the efficiencies of urea mineralization and H_2 generation in aqueous solutions containing 0.1 M NaOH plus 10 mM urea were estimated (and reported in Table 1) by measuring the total organic carbon (TOC) removal and the faradaic efficiency of the H_2 generation (η_{H_2}), before and after 120 min of urea electrolysis (the same experimental window used when preparing Fig. 7) between TiO_2-bearing and non-TiO_2-bearing anodes. During these experiments, where the entire initial TOC (119 ppm) was due to the initial urea concentration, the percentages of TOC removal and values of η_{H_2} after 120 min of urea electrolysis on TiO_2-bearing (23.95%, 0.99) and non-TiO_2-bearing (13.02%, 0.46) anodes

Please cite this article in press as: Murcio-Hernández, S. et al., Electrocatalytic urea mineralization in aqueous alkaline medium using Ni^{II}cyclam-modified nanoparticulate TiO_2 anodes and its relationship with the simultaneous electrogeneration of H_2 on Pt counterelectrodes. Arabian Journal of Chemistry (2018), https://doi.org/10.1016/j.arabjc.2017.12.029

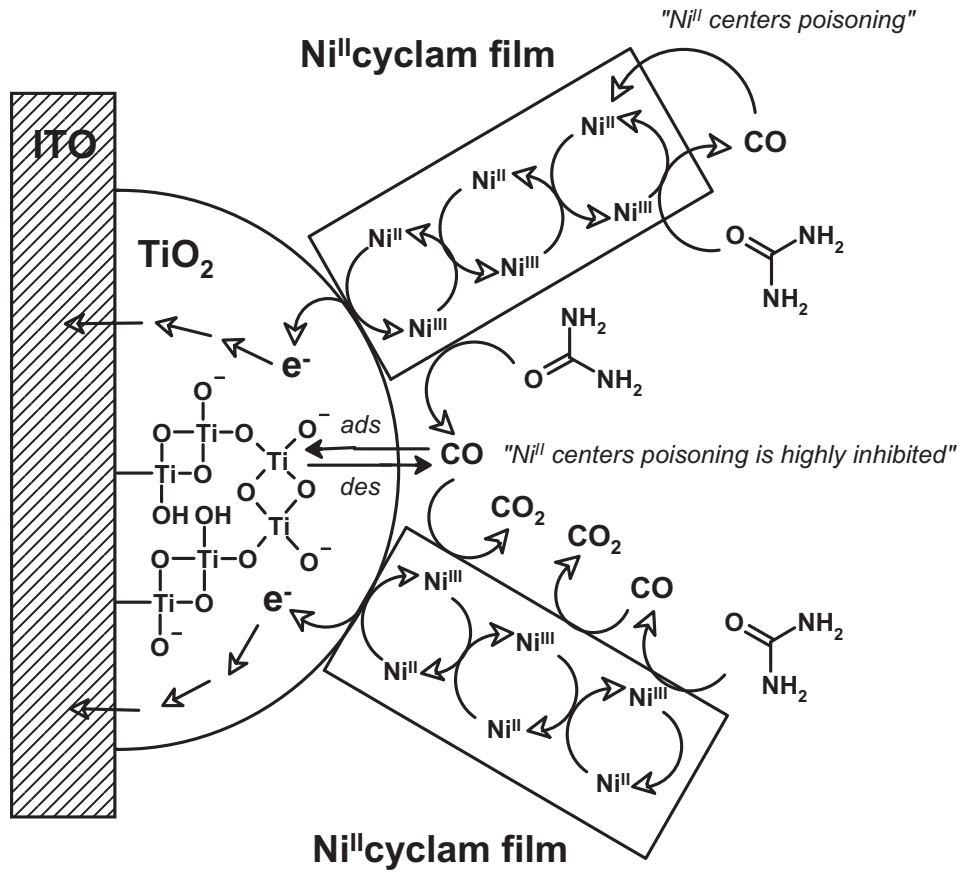

Scheme 6 Representation of the inhibition of the $[O–Ni^{II}L{\sim}Ni^{II}L–O]^{3+}$ centers poisoning during the electrocatalytic urea oxidation on TiO_2-bearing anodes ($ITO/TiO_2//Ni^{II}$cyclam). The inhibition of this phenomenon is promoted by adsorption/desorption phenomena of CO molecules on the nanoparticulate TiO_2 coatings (at Ti^{3+} donor sites).

Table 1 Total organic carbon (TOC) removal and faradaic efficiencies of the H_2 generation (η_{H_2}) after 60 and 120 min of urea electrolysis on TiO_2-bearing anodes ($ITO/TiO_2//Ni^{II}$-cyclam) and non-TiO_2-bearing anodes ($ITO//Ni^{II}$cyclam). See Supplementary Data SD-7 for more details about the estimation of η_{H_2}.

Anode	Urea electrolysis time (min)	TOC removal (%)	η_{H_2} on Pt cathode
$ITO/TiO_2//$ Ni^{II}cyclam	60	8.40	0.57
	120	23.95	0.99
$ITO//$ Ni^{II}cyclam	60	9.66	0.51
	120	13.02	0.46

confirmed that the urea mineralization and the H_2 production were about twice as effective with the TiO_2 nanoparticles present than without them. Confirming that selective adsorption of a high interfacial concentration of CO intermediates on the TiO_2 nanoparticles helps inhibit the poisoning of $[O–Ni^{II}L{\sim}Ni^{II}L–O]^{3+}$ centers (Eq. (17)), improving the CO_{ads} conversion to CO_2 (Eq. (16)) and urea mineralization. In contrast, at shorter electrolysis time (< 60 min) when the interfacial concentration of CO intermediates is significantly lower, their conversion to CO_2 (Eq. (16)) is not preferential as the levels of urea mineralization would also be low. Therefore, the percentages of TOC removal and the values of η_{H_2} (up to 60 min of urea electrolysis in Table 1) showed comparable performances for either $ITO/TiO_2//Ni^{II}$cyclam (8.40%, 0.57) or $ITO//Ni^{II}$-cyclam (9.66%, 0.51) anodes.

A final comparison between our results and those reported in selected publications (see Table 2) reveals that the Ni^{II}-cyclam-modified nanoparticulate TiO_2-coated ITO anodes here developed constitutes a promising electrocatalytic system for performing direct urea mineralization at a relative short electrolysis time. Furthermore, the combination of the following phenomena: (a) effective charge separation on the semiconducting ITO|nanoparticulate TiO_2 junctions, (b) remarkable capabilities of the nanoporous TiO_2 films for tuning the load of OH^- anions demanded by the urea oxidation and, (c) outstanding capabilities of the TiO_2 nanoparticles for capturing CO intermediates (at Ti^{3+} donor sites), successfully promoted the enhancement of the electron external transport to Pt cathodes, and consequently improved the faradaic efficiency associated to the cathodic generation of H_2.

Please cite this article in press as: Murcio-Hernández, S. et al., Electrocatalytic urea mineralization in aqueous alkaline medium using Ni^{II}cyclam-modified nanoparticulate TiO_2 anodes and its relationship with the simultaneous electrogeneration of H_2 on Pt counterelectrodes. Arabian Journal of Chemistry (2018), https://doi.org/10.1016/j.arabjc.2017.12.029

Table 2 Selected publications of electrocatalytic materials for urea electrolysis and H_2 evolution reactions. The results obtained in this work were inserted for comparison purposes.

References	Key electrode materials	Test conditions	Efficiency of anodic urea mineralization (%)	Faradic efficiency of cathodic generation of H_2
Boggs et al. (2009)	Anode: NiO(OH) Cathode: Policrystalline Pt	Aqueous 5 M NaOH + 0.33 M urea at 25 °C 22 h-electrolysis	13	Not reported
Kim et al. (2013)	Anode: Bi-doped TiO_2 (BiO_x/TiO_2) Cathode: Stainless steel (SS)	Aqueous 50 mM NaCl + 33 mM urea at room temp. 0.66 h-electrolysis	80	0.1
Cho and Hoffmann (2014)	Anode: Bi-doped TiO_2 (BiO_x/TiO_2). Cathode: Stainless steel (SS)	Aqueous 50 mM NaCl + 41.6 mM urea at room temp. 6 h-electrolysis	77	Not reported
Liu et al. (2017)	Anode: Ni_2P-modified carbon cloth (CC/Ni_2P). Cathode: ídem	Aqueous 1 M KOH + 0.5 M urea at 25 °C 1 h-electrolysis	Not reported	1.00
This work	Anode: Ni^{II}cyclam-modified nanoparticulate TiO_2 (ITO/TiO_2//Ni^{II}cyclam) Cathode: Polycrystalline Pt	Aqueous 0.1 M NaOH + 10 mM urea at 25 °C 2 h-electrolysis	23.95	0.99

4. Conclusions

Ni^{II}cyclam-modified nanoparticulated TiO_2-coated ITO electrodes (system **ITO/TiO_2//Ni^{II}cyclam**) were successfully prepared. They appeared to inhibit the poisoning of Ni^{II} centers in the presence of an excess of CO intermediates, which were continuously produced during urea oxidation. For comparison, the details of the urea oxidation process was also studied on Ni^{II}cyclam-modified ITO electrodes (system **ITO//Ni^{II}-cyclam**). During testing, the urea mineralization on the TiO_2-bearing anodes (23.95% − TOC removal at 120 min of electrolysis) was twice as effective than the experiment using non-TiO_2-bearing anodes (13.02% − TOC removal at 120 min of electrolysis). This was because the CO intermediates produced during urea oxidation could be selectively adsorbed (or captured) on the nano-TiO_2 surface before the interaction with Ni^{II} centers was established. Following these findings, the faradaic efficiency of the H_2 generation from the H_2O reduction on a Pt cathode electrically connected to TiO_2-bearing anodes (η_{H_2} = 0.99 at 120 min of electrolysis), was also twice as effective when the same Pt cathode was electrically connected to non-TiO_2-bearing anodes (η_{H_2} = 0.46 at 120 min of electrolysis).

The preparation procedure for the Ni^{II}cyclam-modified nanoparticulate TiO_2-coated ITO electrodes here presented, suggests an unexplored approach to obtain promising chemically-modified electrodes for conducting: (a) mineralization of aqueous urea (assisted by the effective inhibition of Ni^{II} centers poisoning by CO intermediates) and, (b) the simultaneous and enhanced generation of electrolytic grade H_2 as a high value-added secondary product.

Acknowledgements

The authors thank the Mexican Council for Science and Technology (CONACyT) for its financial support of this work (grant 258789). S.M.H., J.A.B.A. and C.G.N. acknowledge CONACyT for their PhD scholarships (grants 232885, 405801 and 332650, respectively). A.V.R.S. also acknowledges CONACyT for her MSc scholarship (grant 714044). The authors thank to Richard R. Lindeke, PhD (Professor Emeritus, MIE@UMD United States of America and Peace Corps volunteer Mexico) for the editing service in English language of this paper. The authors thank to Prof. Luis A. Godínez, Prof. José de Jesús Pérez-Bueno and Lib. Ma. Isabel Mendoza-Hernández (CIDETEQ) for all the facilities that supported this work. The author also thanks to Prof. Marino Dávila (BUAP, México) for all his valuable comments about the experimental results of this project.

Appendix A. Supplementary material

Supplementary data associated with this article can be found, in the online version, at https://doi.org/10.1016/j.arabjc.2017.12.029.

Please cite this article in press as: Murcio-Hernández, S. et al., Electrocatalytic urea mineralization in aqueous alkaline medium using Ni^{II}cyclam-modified nanoparticulate TiO_2 anodes and its relationship with the simultaneous electrogeneration of H_2 on Pt counterelectrodes. Arabian Journal of Chemistry (2018), https://doi.org/10.1016/j.arabjc.2017.12.029

References

Acevedo-Peña, P., Manríquez, J., González, I., 2010. ECS Trans. 9, 183–192.
Alatorre-Ordaz, A., Bedioui, F., Gutiérrez-Grandos, S., 1998. Bol. Soc. Chil. Quim. 43, 375–390.
Amstutz, V., Katsaounis, A., Kapalka, A., Comninellis, C., Udert, K. M., 2012. J. Appl. Electrochem. 42, 787–795.
Boggs, B.K., King, R.L., Botte, G.G., 2009. Chem. Comm., 4859–4861
Bosnich, B., Tobe, M.L., Webb, G.A., 1965. Inorg. Chem. 4, 1109–1112.
Boukamp, B.A., Bouwmeester, H.J.M., 2003. Solid State Ionics 157, 29–33.
Boukamp, B.A., Verbraeken, M., Blank, D.H.A., Holtappels, P., 2006. Solid State Ionics 177, 2539–2541.
Bratsch, S.G., 1989. J. Phys. Chem. Ref. Data 18, 21.
Bukowska, J., Roslonek, G., Taraszewska, J., 1996. J. Electrochem. Soc. 403, 47–52.
Cao, F., Oskam, G., Searson, P.C., Stipkala, J.M., Heimer, T.A., Farzad, F., Meyer, G.J., 1980. J. Phys. Chem. 99 (1995), 11974–11981.
Casella, I.G., Cataldi, T.R.I., Salvi, A.M., Desimoni, E., 1993. Anal. Chem. 65, 3143–3150.
Chen, A., La Russa, D.J., Miller, B., 2004. Langmuir 20, 9695–9702.
Cho, K., Hoffmann, M.R., 2014. Environ. Sci. Technol. 48, 11504–11511.
Chowdhury, F.R., Chowdhury, S., Hasan, F., Begum, T., 2011. J. Blangladesh Acad. Sci. 35, 99–111.
Ciszewski, A., Miczarek, G., 1999. J. Electroanal. Chem. 469, 18–26.
Climent, V., Rodes, A., Orts, J.M., Feliu, J.M., Pérez, J.M., Aldaz, A., 1997. Langmuir 13, 2380–2389.
Climent, V., Rodes, A., Albalat, R., Claret, J., Feliu, J.M., Aldaz, A., 2001. Langmuir 17, 8260–8269.
Daramola, D.A., Singh, D., Botte, G.G., 2010. J. Phys. Chem. B 14, 11513–11521.
Daubinger, P., Kieninger, J., Unmüssig, T., Urban, G.A., 2014. Phys. Chem. Chem. Phys. 16, 8392–8399.
Díaz-Morales, O., Ferrus-Suspendra, D., Koper, M.T.M., 2016. Chem. Sci. 7, 2639–2645.
Fabregat-Santiago, F., Garcia-Belmonte, G., Bisquert, J., Bogdanoff, P., Zaban, A., 2003. J. Electrochem. Soc. 150, E293–E298.
Fernández-Nieves, A., Richter, C., de las Nieves, F.J., 1998. Progr. Colloid Polym. Sci. 110, 21–24.
Ferrer, S.J., Gutierrez-Granados, S., Bediou, F., Alatorre-Ordaz, A., 2003. Electroanalysis 15, 70–73.
Fleischmann, M., Korinek, K., Pletcher, D., 1971. J. Electroanal. Chem. 31, 39–49.
Gagné, R.R., Ingle, D.M., 1981. Inorg. Chem. 20, 420–425.
Gu, X., Li, X., Wu, S., Shi, J., Jiang, G., Jiang, G., Tian, S., 2016. RCS Adv. 6, 8070–8078.
Guo, F., Ye, K., Cheng, K., Wang, G., Cao, D., 2015. J. Power Sources 278, 562–568.
Hassanzadeh, A., Habibi, M.H., Zeini-Isfahani, A., 2004. Acta Chim. Slov. 51, 507–527.
Heimer, T.A., Bignozzi, C.A., Meyer, G.J., 1994. J. Phys. Chem. 97 (1993), 11987–11991.
Hernlem, B.J., 2005. Water Res. 39, 2245–2252.
Huang, W., Li, Z., Peng, Y., Niu, Z., 2004. Chem. Commun., 1380–1381
Kim, J., Monllor-Satoca, D., Choi, W., 2012. Energy Environ. Sci. 5, 7647–7656.
Kim, J., Choi, W.J.K., Choi, J., Hoffmann, M.R., Park, H., 2013. Catal. Today 199, 2–7.
King, R.L., Botte, G.G., 2011. J. Power Sources 196, 2773–2778.
King, R.L., Botte, G.G., 2011. J. Power Sources 196, 9579–9584.
Kozitsina, A.N., Shalygina, Zh.V., Dedeneva, S.S., Rusinov, G.L., Toshchina, S.G., Verbitskiy, E.V., Brainina, Kh.Z., 2009. Russian Chem. Bull. Int. Ed. 58, 1119–1125.
Kozuka, H., Takahashi, Y., Zhao, G., Toko, T., 2000. Thin Solid Films 358, 172–179.
Liang, Y., Liu, Q., Asiri, A.M., Sun, X., 2015. Electrochim. Acta 153, 456–460.
Liu, S.-J., 2004. Electrochim. Acta 49, 3235–3241.
Liu, D., Liu, T., Zhang, L., Qu, F., Du, G., Asiri, A.M., Sun, X., 2017. J. Mater. Chem. A 5, 3208–3213.
Liu, Q., Xie, L., Qu, F., Liu, Z., Du, G., Asiri, A.M., Sun, X., 2017. Inorg. Chem. Front. https://doi.org/10.1039/C7QI00185A. Advance Article.
Lustemberg, P.G., Scherlis, D.A., 2013. J. Chem. Phys. 138, 124702 (8 pages).
Malinski, T., Ciszewski, A., Bennett, J., Fish, J.R., Czuchajowski, L., 1991. J. Electrochem. Soc. 138, 2008–2015.
Manriquez, J., Bravo, J.L., Gutierrez-Granados, S., Sucar Succar, S., Bied-Charreton, C., Alatorre-Ordaz, A., Bediou, F., 1999. Anal. Chim. Acta 378, 159–168.
Manríquez, J., Godínez, L.A., 2007. Thin Solid Films 515, 3402–3413.
McAuley, A., Xu, C., 1992. Inorg. Chem. 31, 5549–5554.
Melle-Franco, M., Pacchioni, G., 2000. Surf. Sci. 54, 54–66.
Miller, A.T., Hassler, B.L., Botte, G.G., 2012. J. Appl. Electrochem. 42, 925–934.
Mueller, R., Kammler, H.K., Wegner, K., Pratsinis, S.E., 2003. Langmuir 19, 160–165.
Pérez-Viramontes, N.J., Méndez, P.F., Díaz-Acosta, C.M., Murcio-Hernández, S., Rodríguez, A., Rodríguez, F.J., Godínez, L.A., Bustos, E., Sepúlveda, S., Manríquez, J., 2014. Electrochim. Acta 143, 247–256.
Pierozynski, B., 2013. Electrocatalysis 4, 37–41.
Pierozynski, B., Morin, S., Conway, B.E., 1999. J. Electroanal. Chem. 467, 30–42.
Plá, C.C., Spada, E.R., Sartorelli, M.L., 2013. Appl. Surf. Sci. 273, 603–606.
Rollinson, A.N., Jones, J., Dupont, V., Twigg, M.V., 2011. Energy Environ. Sci. 4, 1216–1224.
Rosłonek, G., Taraszewska, J., 1992. J. Electroanal. Chem. 325, 285–300.
Rosłonek, G., Taraszewska, J., 1994. Electrochim. Acta 39, 1887–1889.
Sheng, W., Gasteiger, H.A., Shao-Horn, Y., 2010. J. Electrochem. Soc. 157, B1529–B1536.
Simka, W., Piotrowski, J., Nawrat, G., 2007. Electrochim. Acta 52, 5696–5703.
Sophia, S.J., Devi, S., Pandian, K., 2012. Int. J. Electrochem. Sci. 7, 6580–6598.
Sorescu, D.C., Yates Jr., J.T., 1998. J. Phys. Chem. B 102, 4556–4565.
Taraszewska, J., Rosłonek, G., Lampeka, Y.A., Maloshtan, I.M., 1998. J. Electroanal. Chem. 452, 49–56.
Trevin, S., Bedioui, F., Gómez-Villegas, M.G., Bied-Charreton, C., 1997. J. Mater. Chem. 7, 923–928.
Turrión, M., Bisquert, J., Salvador, P., 2003. J. Phys. Chem. B 35, 9397–9403.
Vedharathinam, V., Botte, G.G., 1812. J. Phys. Chem. C 118 (2014), 21806–21812.
Vedharathinam, V., Botte, G.G., 2012. Electrochim. Acta 81, 292–300.
Vedharathinam, V., Botte, G.G., 2013. Electrochim. Acta 108, 660–665.
Wanbayor, R., Deák, P., Frauenheim, T., Ruangpornvisuti, V., 2011. J. Chem. Phys. 134, 104701 (6 pages).
Wang, G., Ling, Y., Lu, X., Wang, H., Qian, F., Tong, Y., Li, Y., 2012. Energy Environ. Sci. 5, 8215–8219.
Wang, D., Yan, W., Botte, G.G., 2011. Electrochem. Commun. 13, 1135–1138.

Please cite this article in press as: Murcio-Hernández, S. et al., Electrocatalytic urea mineralization in aqueous alkaline medium using Ni^{II}cyclam-modified nanoparticulate TiO_2 anodes and its relationship with the simultaneous electrogeneration of H_2 on Pt counterelectrodes. Arabian Journal of Chemistry (2018), https://doi.org/10.1016/j.arabjc.2017.12.029

Wang, D., Yan, W., Vijapur, S.H., Botte, G.G., 2012. J. Power Sources 217, 498–502.
Wang, D., Yan, W., Vijapur, S.H., Botte, G.G., 2013. Electrochim. Acta 89, 732–736.
Yamada, H., Imahori, H., Nishimura, Y., Yamasaki, I., Ahn, T.K., Kim, S.K., Kim, D., Fukuzumi, S., 2003. J. Am. Chem. Soc. 125, 9129–9139.
Yan, W., Wang, D., Botte, G.G., 2012. Appl. Catal. B 127, 221–226.
Zhang, R., Liu, L., Li, Y., Wang, W., Li, R., 2015. Int. J. Electrochem. Sci. 10, 2355–2369.
Zhang, Z., Yates Jr., J.T., 2010. J. Am. Chem. Soc. 132, 12804–12807.

Please cite this article in press as: Murcio-Hernández, S. et al., Electrocatalytic urea mineralization in aqueous alkaline medium using Ni^{II}cyclam-modified nanoparticulate TiO_2 anodes and its relationship with the simultaneous electrogeneration of H_2 on Pt counterelectrodes. Arabian Journal of Chemistry (2018), https://doi.org/10.1016/j.arabjc.2017.12.029